GBE

Comparative Genomics and Phylogenomics of the Mustelinae Lineage (Mustelidae, Carnivora)

Azamat A. Totikov [1,2,*], Andrey A. Tomarovsky [1,2], Polina L. Perelman [1], Tatiana M. Bulyonkova [3], Natalia A. Serdyukova [1], Aliya R. Yakupova [4,5], David Mohr [6], Daniel W. Foerster [7], Jose Horacio Grau Jipoulou [8], Violetta R. Beklemisheva [1], Mikhail Sidorov [9], Inês Miranda [10,11,12], Liliana Farelo [10,12], Alexei V. Abramov [13], Ksenia Krasheninnikova [14], Anna S. Mukhacheva [15], Victor V. Panov [16], Elena Balanovska [17], Nikolay Cherkasov [18], Karol Zub [19], Alan F. Scott [6], José Melo-Ferreira [10,11,12], Innokentiy M. Okhlopkov [9], Anna Zhuk [20,21], Klaus-Peter Koepfli [22], Alexander S. Graphodatsky [1], Sergei Kliver[23]

[1]Laboratory of Diversity and Evolution of Genomes, Institute of Molecular and Cellular Biology SB RAS, Novosibirsk 630090, Russia
[2]Department of Natural Sciences, Novosibirsk State University, Novosibirsk 630090, Russia
[3]Youth Laboratory of Molecular Genetics, Yugra State University, Khanty-Mansiysk 628011, Russia
[4]Division of Evolutionary Biology, Ludwig-Maximilians-Universität, Planegg 82152, Germany
[5]Microevolution and Biodiversity, Max Planck Institute for Biological Intelligence, Seewiesen 82319, Germany
[6]Genetic Resources Core Facility, Department of Genetic Medicine, Johns Hopkins University School of Medicine, Baltimore, MD 21287, USA
[7]Leibniz Institute for Zoo and Wildlife Research (IZW), Berlin 10315, Germany
[8]Smithsonian Conservation Biology Institute, Center for Species Survival, Washington, DC, USA
[9]Institute of Biological Problems of Cryolithozone SB RAS, Yakutsk 677000, Russia
[10]CIBIO, Centro de Investigação em Biodiversidade e Recursos Genéticos, InBIO Laboratório Associado, Universidade do Porto, Vairão 4485-661, Portugal
[11]Departamento de Biologia, Faculdade de Ciências da Universidade do Porto, Porto 4169-007, Portugal
[12]BIOPOLIS Program in Genomics, Biodiversity and Land Planning, CIBIO, Vairão 4485-661, Portugal
[13]Laboratory for Theriology, Zoological Institute RAS, St. Petersburg 199034, Russia
[14]Independent Researcher, Hinxton, Saffron Walden CB10 1RQ, UK
[15]Sikhote-Alin Biosphere Zapovednik, Ternei 692150, Russia
[16]Institute of Systematics and Ecology of Animals SB RAS, Novosibirsk 630091, Russia
[17]Laboratory of Human Population Genetics, Research Centre for Medical Genetics, Moscow 115522, Russia
[18]Centre for Computational Biology, Peter the Great Saint Petersburg Polytechnic University, St. Petersburg 195251, Russia
[19]Mammal Research Institute PAS, Białowieża 17-230, Poland
[20]Institute of Applied Computer Science, ITMO University, St. Petersburg 197101, Russia
[21]Laboratory of Amyloid Biology, St. Petersburg State University, St. Petersburg 199034, Russia
[22]Smithsonian-Mason School of Conservation, Front Royal, VA 22630, USA
[23]Center for Evolutionary Hologenomics, the Globe Institute, The University of Copenhagen, Copenhagen 1353, Denmark

*Corresponding author: E-mail: a.totickov1@gmail.com.

Accepted: January 09, 2026

Abstract

Mustelinae are among the most diverse and taxonomically complex subfamilies within the Mustelidae, yet their evolutionary history and genetic diversity remain largely unexplored at the whole-genome level. Here, we present the first comprehensive comparative and phylogenomic study of this lineage, integrating nuclear and mitochondrial genomes from 10 species across the Holarctic and Indomalayan realms. Our dataset includes two novel genome assemblies (*Mustela strigidorsa*, *M. sibirica*) and an improved genome for *M. nivalis*, enabling robust cross-species analyses of genome size, chromosomal evolution, genetic diversity, and demographic history. We uncover striking inter- and intraspecific variation in genome-wide heterozygosity and genome size, with evidence of marked homozygosity in some Asian lineages (*M. eversmanii*, *M. sibirica*, *M. strigidorsa*) and remarkable genetic diversity in widespread species such as *M. nivalis* and *M. erminea*. Phylogenomic results support the previously suggested split of *M. richardsonii* from *M. erminea*, but we found no evidence for speciation within *M. nivalis*. Ancestral reconstruction of chromosomal rearrangements revealed key chromosomal fissions that shaped the Mustelinae radiation, including early events predating the divergence of modern *Mustela* species. The results confirmed the suggested ancestral karyotypes of *Mustela* ($2n = 44$) and Mustelinae ($2n = 42$). Finally, demographic reconstructions exposed species-specific responses to Quaternary climatic cycles, ranging from long-term resilience in *M. nivalis* to repeated population bottlenecks in *M. putorius* and *M. sibirica*. Collectively, our findings establish a genomic foundation for future evolutionary and conservation genomic research on this emblematic Mustelidae lineage.

Key words: *mustela*, *neogale*, chromosomal evolution, phylogenomics, genetic diversity, demographic history.

Significance

Understanding how weasels and their relatives evolved has long been limited by the lack of comprehensive whole-genome data, leaving open questions about their true species boundaries, chromosome evolution, and genetic diversity across their wide geographic ranges. By integrating nuclear and mitochondrial data across 10 species and generating new reference genomes this study reveals previously unknown patterns of genetic diversity, clarifies long-standing taxonomic uncertainties, and reconstructs key chromosomal changes that shaped the group's evolution. These findings fill major gaps in our knowledge of Mustelinae evolution and provide a genomic foundation essential for future research and conservation planning.

Introduction

The Mustelinae lineage represents the most numerous and diverse group of small mammals within the Mustelidae family, comprising at least 20 recognized species in the genera *Mustela* and *Neogale* (Fig. 1). Their high ecological adaptability has enabled them to inhabit a wide range of environments throughout the Holarctic region (Fig. 1) (Macdonald et al. 2017). While most Mustelinae species inhabit the Palearctic and Nearctic regions, some are restricted to the Neotropics (*N. africana*, *N. felipei*) or the Indomalayan zone (*M. kathiah*, *M. strigidorsa*, *M. nudipes,* and *M. lutreolina*). Many of these species are exploited by humans to varying degrees, whether in the fur industry (*M. sibirica*, *M. putorius*, *M. eversmanii*, *M. erminea*, and *N. vison*), in agriculture for rodent population control (e.g. *M. erminea*), in traditional Asian medicine (e.g. *M. strigidorsa*), as domestic pets, or even as model organisms for studying various viral diseases (*M. putorius furo*) (Belser et al. 2011; Harrington et al. 2017; Hiller and Vantassel 2022).

Research on Mustelinae species has often focused only on describing their morphology, emphasizing physical characteristics such as body size, skull shape, fur patterns, and other distinctive features (Kitchener et al. 2017). However, these studies revealed the challenges of studying this subfamily, with factors such as varying degrees of sexual dimorphism, age-related variability, and the occurrence of interspecific hybrids complicating accurate taxonomic delineation (Kitchener et al. 2017). As a result, researchers increasingly turned to molecular and cytogenetic approaches to gain deeper insight into the evolution of the subfamily. Cytogenetic research elucidated the complex karyotypic evolution in Mustelinae, characterized by multiple chromosomal rearrangements, including fusions that

Fig. 1. Geographic range and global conservation status of Mustelinae species. a–l) Photos of 12 out of the 20 currently recognized Mustelinae species reproduced from Flickr and iNaturalist under Creative Commons licenses: a) Least weasel (*M. nivalis*), Yersinia pestis, Flickr, CC BY-NC-SA; b) Stoat (*M. erminea*), Jing-Yi Lu, iNaturalist, CC BY-NC; c) American ermine (*M. richardsonii*), Vinny Pellegrino, iNaturalist, CC BY-NC; d) Back-striped weasel (*M. strigidorsa*), lordworm_cryptopsy, iNaturalist, CC BY-NC; e) Mountain weasel (*M. altaica*), Li Jianong, iNaturalist, CC BY-NC; f) Black-footed ferret (*M. nigripes*), Tory Mathis, iNaturalist, CC BY-NC; g) Steppe polecat (*M. eversmanii*), Anna Golubeva, iNaturalist, CC BY-NC-ND, reproduced with the permission of the author; h) Siberian weasel *(M. sibirica*), Nazim Ali Khan, iNaturalist, CC BY-NC; i) Yellow-bellied weasel (*M. kathiah*), jbhatia, iNaturalist, CC BY-NC; j) Long-tailed weasel *(N. frenata*), Donna Pomeroy, iNaturalist, CC BY-NC; k) European polecat (*M. putorius*), bandwidthbob, iNaturalist, CC BY-NC; l) American mink (*N. vison*), Tobin Brown, iNaturalist, CC BY-NC. Images were cropped for clarity. m) Geographic range and global conservation status of Mustelinae species. Ranges for *M. richardsonii*, *M. haidarum,* and *M. aistoodonnivalis* are based on previous studies (Colella et al. 2018, 2021; Liu et al. 2023). Ranges for all other species were obtained from the IUCN Red List of Threatened Species (IUCN 2025). Global conservation statuses according to IUCN data: LC, Least Concern, NT, Near Threatened, VU, Vulnerable, EN, Endangered, CR, Critically Endangered, NE, Not Evaluated.

produced the *N. vison* karyotype (2*n* = 30) and both fissions and fusions that generated a karyotype resembling that of *M. erminea* (2*n* = 44) (Graphodatsky et al. 1989). Moreover, substantial differences in the number of chromosomal arms among *Mustela* species, despite similar or identical diploid numbers (2*n*), cannot be explained solely by typical structural rearrangements (Graphodatsky et al. 1989). Karyotype evolution within *Mustela* has involved the emergence of additional, entirely heterochromatic arms in the karyotypes of certain species, through an increase in heterochromatic material on the short arms of originally acrocentric chromosomes (Graphodatsky et al. 2002). While Mustelinae species share some similarities in heterochromatin localization, they differ in the size of heterochromatic blocks and, consequently, in total heterochromatin content, which affects the genome size (Graphodatsky et al. 1977). These and other cytogenetic studies have laid the groundwork for understanding the complex phylogenetic relationships within this diverse group of mammals. Notably, even before the advent of sequencing technologies, cytogenetic studies had already indicated the need to separate *Neogale* from *Mustela* within the Mustelinae subfamily (Graphodatsky et al. 1989).

In recent decades, the systematics of Mustelidae species has undergone significant revisions and changes, primarily based on nuclear and/or mitochondrial data (Koepfli et al. 2008a; Yu et al. 2011; Sato et al. 2012; Law et al. 2018; Hassanin et al. 2021). Stepping beyond morphological markers has enabled a reevaluation of the traditional taxonomy of Mustelidae (Simpson 1945), leading to the division of the five previously recognized subfamilies into eight (Koepfli et al. 2008a; Yu et al. 2011). Subsequent studies focusing on Mustelinae, along with extensive discussions (Harding and Smith 2009; Hassanin et al. 2021; Patterson et al. 2021, 2025), helped to refine the boundaries between the genera *Mustela* and *Neogale*. Species-level classification remains challenging due to the rapid evolutionary diversification within this group (Koepfli et al. 2008b; Law et al. 2018; Hassanin et al. 2021), which has resulted in a number of morphologically indistinguishable species, as well as hard-to-resolve nodes on phylogenetic trees (Koepfli et al. 2008a). This complexity is further exacerbated by hybridization among some species (Cabria et al. 2011; Cserkész et al. 2021), which often leads to ambiguous phylogenetic relationships (Etherington et al. 2022). Uncertainty over species boundaries contributes to the lack of consensus on the total number of species or subspecies within Mustelinae. Despite these difficulties, a notable taxonomic revision has been the recognition of *M. itatsi* as taxonomically distinct from the closely related *M. sibirica*, previously classified as a single species (Abramov 2000). Similarly, taxonomic reassessment has successfully resolved the classification of *M. erminea.* Whole-genome and mitochondrial data (Colella et al. 2018, 2021) revealed that North American *M. erminea* actually comprises three distinct species: *M. erminea*, *M. richardsonii,* and *M. haidarum*. *M. nivalis*, the least weasel, has a similar range as ermines, but is still considered to be a single species. Multiple studies report a notable variation of phenotypic traits, eg, of body length and mass, coloration, and craniological metrics, but researchers do not agree on the number of subspecies (McDevitt et al. 2013; Vass and Bende 2023). Moreover, a recent phylogeographical study based on four mitochondrial and nuclear markers showed presence of two major clades correlated with the coat coloration, but have not reliably resolved low-level structure (Sato et al. 2020). These facts make a hypothesis of a species complex within *M. nivalis* deserving consideration and evaluation on the genomic level.

Currently, mitochondrial genome assemblies are available for nearly every species within the Mustelinae, with the exception of *M. lutreolina*, and *M. aistoodonnivalis*. However, the availability of whole-genome data is far less complete. Genome assemblies are absent for thirteen species (*M. strigidorsa*, *M. sibirica*, *M. altaica*, *M. aistoodonnivalis*, *M. itatsi*, *M. kathiah*, *M. lutreolina*, *M. nudipes*, *M. haidarum*, *M. richardsonii*, *N. frenata*, *N. felipei,* and *N. africana*). Among the remaining species, chromosome-level genome assemblies were published for only six species (*M. nivalis*, *M. erminea*, *M. lutreola*, *M. nigripes*, *M. putorius furo,* and *N. vison*), and scaffold-level genome assemblies exist for only two others (*M. eversmanii* and *M. putorius*). Notably, the genome assembly for *M. nivalis* was published very recently (O'Brien et al. 2025). Despite the increasing volume of available genomic data, its distribution across the Mustelinae lineage remains uneven (Table S1), underscoring the need for further sequencing and genome assembly efforts for the less-studied species.

Comparative analysis based on the integration of nuclear and mitochondrial genome data represents a powerful tool for studying evolutionary processes, enabling the identification of both common features and key differences between related species. This approach is particularly significant in the context of conservation research, where understanding genetic diversity, phylogenetic relationships, and demographic history is crucial for developing effective biodiversity conservation strategies. In this study, we compiled an extensive dataset, comprising 10 genome assemblies, 50 resequencing samples, and 149 mitochondrial genomes. This dataset includes three new genomic assemblies, two of which were generated by us and one improved from a publicly

available draft genome assembly, as well as 9 samples newly resequenced as part of this project. Using this comprehensive dataset, we aimed to: (i) evaluate genome size variation within and between species; (ii) determine interspecific and intraspecific phylogenetic relationships; (iii) reconstruct synteny blocks to identify structural rearrangements among genomes; (iv) assess and compare genetic diversity among the species on the whole-genome level; and (v) reconstruct population history. Thus, our study contributes to a deeper understanding of genetic diversity and evolutionary processes within the Mustelinae, while also offering valuable guidance for the development of conservation strategies and the preservation of genetic diversity in these species.

Results

Two New Chromosome-level Genome Assemblies

We improved the previously published draft genome assembly of *M. nivalis* (GCA_019141155.1) (Miranda et al. 2021) to chromosome-level and generated the first chromosome-level assembly for *M. strigidorsa*. The *M. nivalis* assembly includes 21 chromosomal scaffolds (Fig. S1a), which correspond to the published karyotype ($2n = 42$) (Graphodatsky et al. 2020), and chromosome numbering follows this karyotype (Table S2). For *M. strigidorsa* we observed $2n = 44$, similar to *M. erminea* (Fig. S1b) (Graphodatsky et al. 2020); this difference is explained by a fusion of chr14 and chr16 in *M. nivalis* (Fig. S1c). A one-to-one synteny between *M. strigidorsa* and *M. erminea* chromosome scaffolds was observed (Fig. S1c); thus we decided to use the same chromosome numbering for both species (Table S3).

The genome assemblies of *M. strigidorsa* and *M. nivalis* have total lengths of 2.42 Gbp and 2.45 Gbp, respectively (Table S4). Notably, the assembly lengths differ from the genome size estimates based on 23-mers: 3.21 Gbp for *M. nivalis* and 3.34 Gbp for *M. strigidorsa* (Table S5). The assembly lengths are comparable to the lengths of other species assemblies included in our study, ranging from 2.41 Gbp for the *M. sibirica* to 2.68 Gbp for the *N. vison*. The scaffold N50 s, 115.1 Mbp (*M. strigidorsa*) and 138.4 Mbp (*M. nivalis*) are also comparable to the values for other Mustelinae assemblies (130.15–220.3 Mbp). The BUSCO analysis using the Mammalia odb10 dataset (2024 to 2001-08, total BUSCOs = 9226) on the obtained genome assemblies of *M. strigidorsa* and *M. nivalis* showed 94.6% and 96% complete and single-copy BUSCOs, with only 3.9% and 2.9% missing BUSCOs, respectively, which is similar to other Mustelinae assemblies (Fig. S2, Table S6).

Genome Size Variation in Mustelinae Species

We observed significant variation of genome sizes across the analyzed species and samples (Fig. 2, Table S5). The estimates ranged from 2.16 Gbp for *M. putorius* (ERR7260426) to 3.35 Gbp for *M. nivalis* (T100). The greatest variation was detected within *M. putorius* and *M. richardsonii*. The *M. putorius* samples formed two distinct groups: one ranging from 2.16 Gbp to 2.3 Gbp and another from 2.53 Gbp to 2.63 Gbp. Among *M. richardsonii* samples, one outlier exhibited a notably small genome size of 2.29 Gbp, while the remaining samples ranged from 2.58 Gbp to 2.79 Gbp. The smallest differences in genome size were observed between *N. vison* individuals. An analysis of Transposable Elements (TE) in the genome assemblies revealed TE content ranging from 35.85% to 39.6% (Table S7). Most TEs belonged to the SINE and LINE superfamilies. Minimal SINE and LINE content were observed in the *M. putorius furo* genome with 9.61% and 19.02%, respectively. Kimura distance-based copy divergence profiles showed similar patterns (same number and location of the peaks) for assemblies across the seven species which included three or more individuals (Fig. S3).

Genome Synteny and Rearrangements

We reconstructed a macro-level synteny map for the available genomes of the Mustelinae as well as other species within the Mustelidae family (Fig. 3). This revealed highly conserved syntenic segments, mostly maintaining centromere positions across species. However, some exceptions indicate evolutionary shifts in centromere positions within the genus *Mustela*. For example, centromere positions in homologous chromosomes of *M. strigidorsa* and *M. erminea* differ from those in other *Mustela* species (Fig. S4). A centromeric shift was observed for MERM 12 and its homologs (Fig. S4a): MSTR 12 and MERM 12 are acrocentrics, whereas MNIV 13, MLUT 9, MPFUR 10 and MNIG 9 are submetacentrics. A similar pattern transformed subtelocentric MSTR 5 and MERM 5 to acrocentric MNIV 17 and MLUT 13, or even to acrocentric MPFUR 16 and MNIG 13 (chromosome numbers are used throughout). Notably, these shifts occurred without accompanying structural rearrangements (Fig. S4b).

Despite these generally conserved patterns, we identified a number of structural rearrangements in *Mustela* genomes, including new inversions (Fig. 3, red connectors) and all previously described Robertsonian translocations (blue connectors). Some of the inversions are likely lineage-specific. For example, inversions between MNIV 12, 13 and 15, and their homologs MLUT 15, 9 and 10 likely distinguish the ferret-like (MLUT, MPFUR,

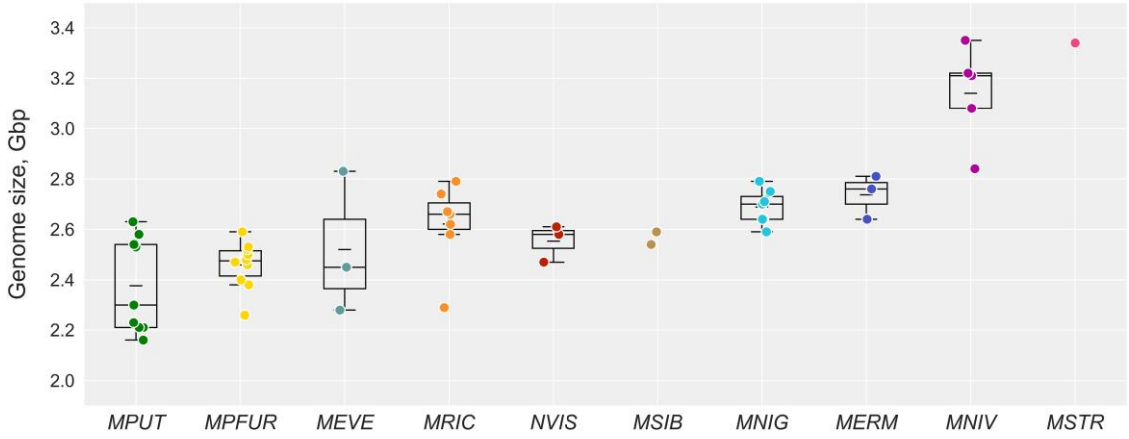

Fig. 2. Estimation of genome sizes for Mustelinae species based on k-mer analysis. Short horizontal lines within boxplots represent the mean value, and long lines indicate the median value. Species abbreviation: MPUT, *Mustela putorius*, MPFUR, *Mustela putorius furo*, MEVE, *Mustela eversmanii*, MRIC, *Mustela richardsonii*, NVIS, *Neogale vison*, MSIB, *Mustela sibirica*, MNIG, *Mustela nigripes*, MERM, *Mustela erminea*, MNIV, *Mustela nivalis*, MSTR, *Mustela strigidorsa*. Detailed data are provided in Table S5.

MNIG) lineage from other *Mustela* species (MSTR, MERM, MNIV). The sizes of these inversions are approximately 6.89 Mbp, 2.23 Mbp, and 13.19 Mbp. At the same time, NVIS stands out due to numerous translocations and species-specific inversions, even if multiple fissions and fusions of chromosomes are not considered. Expectedly, distinct heterochromatic arms observed in cytogenetic studies on the chromosomes of some *Mustela* species (Graphodatsky et al. 1976, 1977, 1989, 2002) are absent in current genome assemblies, which is evident from the reconstructed syntenic blocks. For instance, the large heterochromatic arm on MNIV 1 and MERM 9 is missing.

Phylogenomics and Karyotype Evolution of Mustelinae

We first reconstructed a whole-genome phylogeny for the lineage and then integrated these results with aforementioned genome synteny analysis. We generated a ML (Maximum Likelihood) phylogenetic tree using positions that vary between species (including heterozygous ones) from 6,599 single-copy protein-coding genes (Fig. 4a). The inferred topology showed a clear differentiation of the currently recognized species. Just as expected, *N. vison* appeared as a sister group to the genus *Mustela*. *M. strigidorsa*, the only tropical species involved in the analysis, diverged first within *Mustela*. Next, stoats (*M. richardsonii* and *M. erminea*), *M. nivalis, M. sibirica, M. lutreola* and, finally, the ferret lineage (*M. eversmannii*, *M. nigripes*, *M. putorius* + *M. p. furo*) split sequentially from the stem. To verify the concatenated ML tree, we reconstructed a coalescent-based phylogeny (Fig. S5), and got a completely congruent topology. All internal nodes at and above the species-level showed high posterior probabilities (pp1 = 1.0). However, quartet support values (q1) varied across the tree (Fig. S6, Table S8). The lowest support was observed for node 9 (Most Recent Common Ancestor (MRCA) of *M. sibirica* and *M. lutreola)*, with only 47.7% of quartets supporting the main topology (q2 = 30.2%, q3 = 21.9%). A higher, but still reduced, quartet support was detected for node 2 (q1 = 61.7%), which corresponds to the MRCA of the *Mustela* and *Neogale* (*N. vison*). All other interspecific nodes were supported by a high fraction of the quartets (q1 = 72.8% to 88.7%).

To trace the evolutionary history and reconstruct ancestral states of the detected Robertsonian translocations, we encoded them as fissions or fusions relative to the *M. strigidorsa* genome (Fig. S7), for example, fis(MSTR8, MSTR15) and fus(MSTR8, MSTR13), and mapped them onto the phylogenetic tree (Fig. 4a). We got consistent results with a previous cytogenetic study (Graphodatsky et al. 2002). However, inclusion of the *M. strigidorsa* assembly, generated in this study, resulted in a better relative placement of the fission event fis(MSTR2; MSTR21). Specifically, while the earlier study suggested that fis(MSTR2; MSTR21) occurred after the divergence of *Neogale* but before the split of *M. erminea*, our phylogenetic placement of *M. strigidorsa*, as a basal lineage within *Mustela*, indicates that the event likely occurred even earlier, prior to the diversification of extant *Mustela* species.

Taxonomic Uncertainties Within Mustelinae

Two species within *Mustela* are both widespread and taxonomically challenging: *M. erminea* and *M. nivalis*. Mitochondrial data have indicated that North

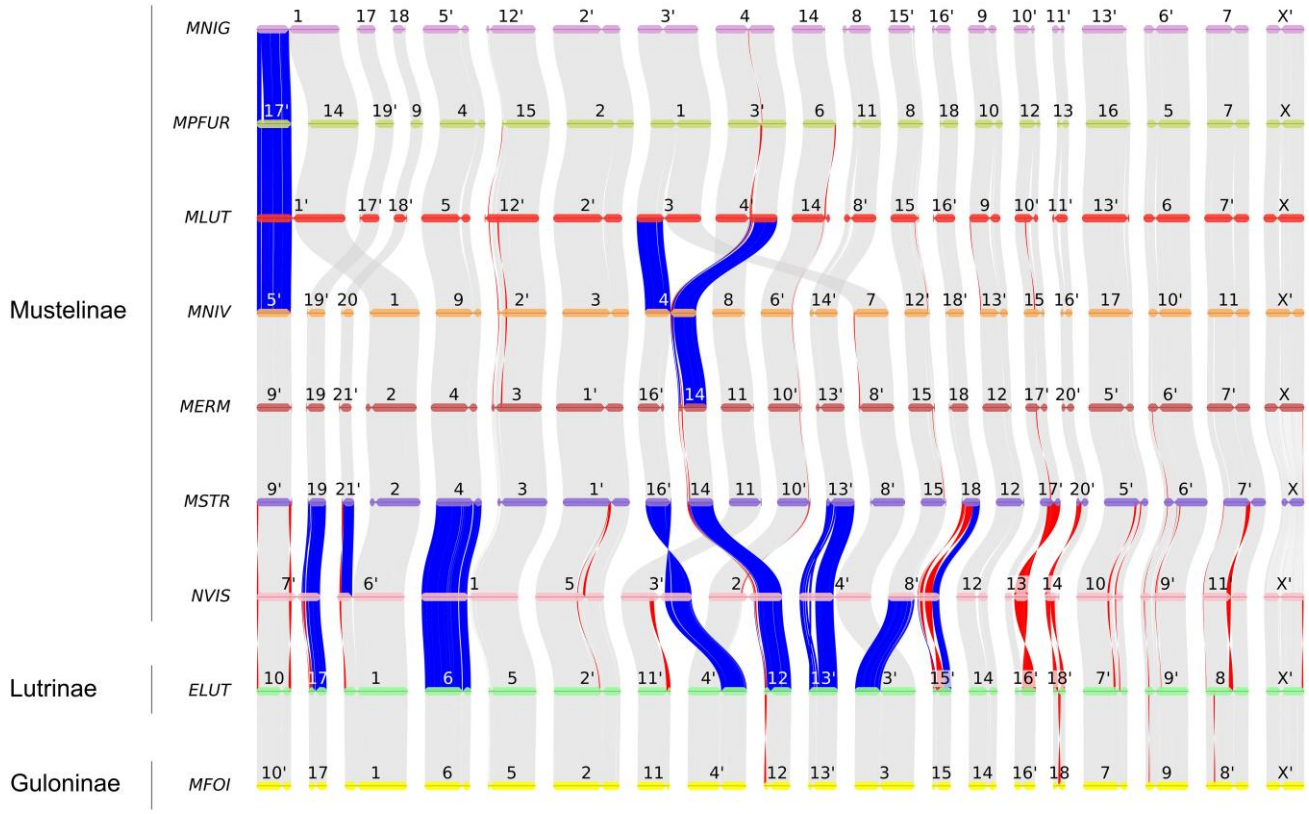

Fig. 3. Macro-level synteny map among species within the mustelinae and mustelidae. Chromosomes labeled by primes (′) were reverse complemented. Fusions and fissions are highlighted in blue. Inversions larger than 1 Mbp are highlighted in red. Macro-level synteny (gray lines) is shown between chromosomes (horizontal colored lines) of seven species of Mustelinae, one Lutrinae (ELUT), and one Guloninae (MFOI) species. Centromeric positions are tentative, approximately drawn based on the analysis of comparative chromosome painting maps and G-banded karyotypes. Abbreviation: MFOI, *Martes foina*, ELUT, *Enhydra lutris*, NVIS, *Neogale vison*, MSTR, *Mustela strigidorsa*, MERM, *Mustela erminea*, MNIV, *Mustela nivalis*, MLUT, *Mustela lutreola*, MPFUR, *Mustela putorius furo*, MNIG, *Mustela nigripes*.

American *M. erminea* includes multiple species (Colella et al. 2021), but the reliance on mtDNA is complicated by frequent hybridization among Mustelinae. Although mitochondrial (Fig. S8) and nuclear trees (Fig. 4a) are largely congruent, we detected clear cases of mitonuclear discordance: the mitochondrial genome PQ821906 of *M. eversmanii* sample ERR11751895 (male) clusters with *M. putorius* in the mitochondrial tree, and sample ERR7260426, identified as *M. putorius* (male), carries *M. lutreola* mtDNA (BK069848). Such discordance limits the significance of mitochondrial data for Mustelinae and emphasizes the need for genome-wide analyses. Given this, we assessed species delimitation in *M. erminea* using genome-wide data and applied the same approach to *M. nivalis*, where species-level divergence has not yet been rigorously tested. To test the hypothesis that there is species-level divergence within *M. nivalis*, we compared genetic distances between and within sister species (Fig. S9): *M. nivalis* (9.77×10^{-4}–1.16×10^{-3}), *M. erminea* (1.08×10^{-3}–1.19×10^{-3}), *M. richardsonii* (1.47×10^{-3}–1.66×10^{-3}), *M. eversmanii* (5.56×10^{-4}–9.12×10^{-4}), *M. erminea-M. richardsonii* (2.30×10^{-3}–2.66×10^{-3}) and *M. eversmanii-M. nigripes* (2.60×10^{-3}–2.80×10^{-3}). We found a clear differentiation between inter- and intraspecific genetic distances (Fig. 4b). Distances within *M. nivalis* are relatively small and clearly fall within the intraspecific category: its mean (1.05×10^{-3}) does not significantly differ from the *M. erminea* mean (1.15×10^{-3}, two-sided Mann-Whitney test p-value 0.095) and is smaller than the mean for *M. richardsonii* (1.15×10^{-3}, one-sided Mann-Whitney test *P*-value = 0.00068). At the same time, our comparison confirms the previous split of *M. richardsonii* and *M. erminea* as the mean distance between them is similar to the distance between *M. eversmanii* and *M. nigripes* (2.47×10^{-3} vs. 2.72×10^{-3}).

Genetic Diversity and Demographic Histories

To investigate how past demographic processes have shaped contemporary genomic variation, we integrated

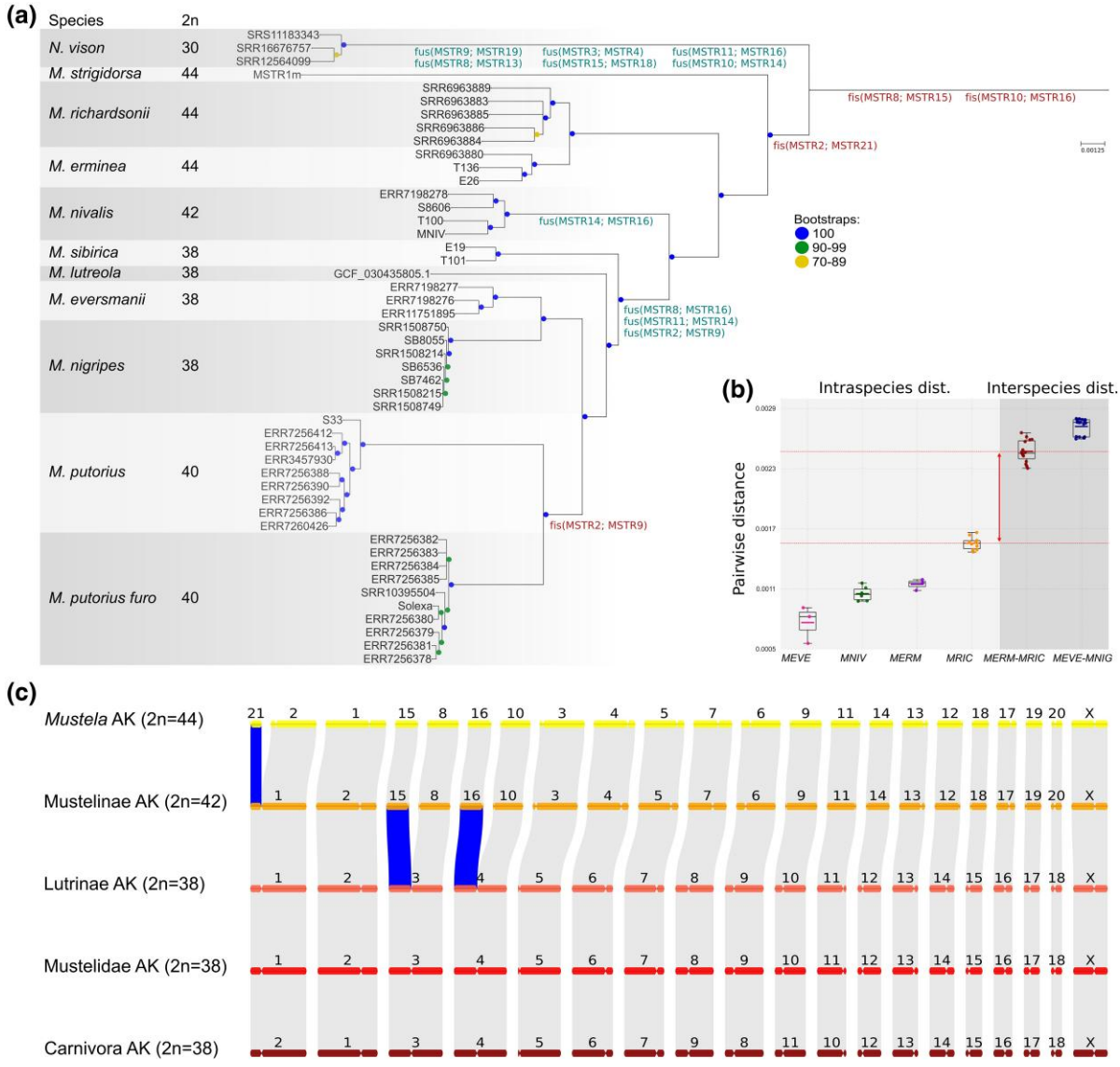

Fig. 4. Phylogenomic relationships, genetic distances, and ancestral karyotype reconstruction in mustelinae. a) Maximum likelihood phylogram based on nuclear phylogenomic data of analyzed Mustelinae species. Only autosome data were used for the reconstruction, and the tree was rooted on *Martes foina* (not shown, mfoi.min_150.pseudohap2.1_HiC, DNA Zoo). Labels near branches correspond to ancestral fissions (red) and fusions (green). The translocations were encoded relative to *M. strigidorsa* chromosomes, as they represent the chromosome-level syntenic blocks. Note a difference in designation between fissions and fusions. For example, fis(MSTR8, MSTR15) means a fission of ancestral chromosome to homologs of MSTR8 and MSTR15, and fus(MSTR14; MSTR16) means a fusion of homologs of MSTR14 and MSTR16 to a new chromosome. b) Intraspecific and interspecific pairwise distances among Mustelinae species. Colored and black horizontal lines within each boxplot represent the mean and median values, respectively. Red dashed lines and arrows indicate the gap between intra- and interspecific distances. Species abbreviation: MEVE – *Mustela eversmanii*, MNIV – *Mustela nivalis*, MERM – *Mustela erminea*, MRIC – *Mustela richardsonii*, MNIG – *Mustela nigripes.* c) The chromosomal synteny (scheme) between ancestral karyotypes (AK) of Carnivora, Mustelidae, Lutrinae, Mustelinae and *Mustela*. Fissions are highlighted in blue. Chromosome numbering for Mustelidae AK and Lutrinae AK is based on that of *Martes foina*, for Carnivora AK we followed the previously proposed nomenclature (Beklemisheva et al. 2016), for Mustelinae AK we used *M. strigidorsa* nomenclature with modification for chr 1 and 2, and for *Mustela* AK it completely corresponds to *M. strigidorsa*.

analyses of heterozygosity (Fig. 5, Table S9), Runs of Homozygosity (RoH) (Fig. 6, Table S10), and historical effective population size (N_e) (Fig. 7) inferred with the Pairwise Sequentially Markovian Coalescent (PSMC) model (Li and Durbin 2011). We detected significant variation in mean heterozygosity (SNP/kbp) both among and within species. Taxa sampled across broad geographic ranges showed the largest intraspecific

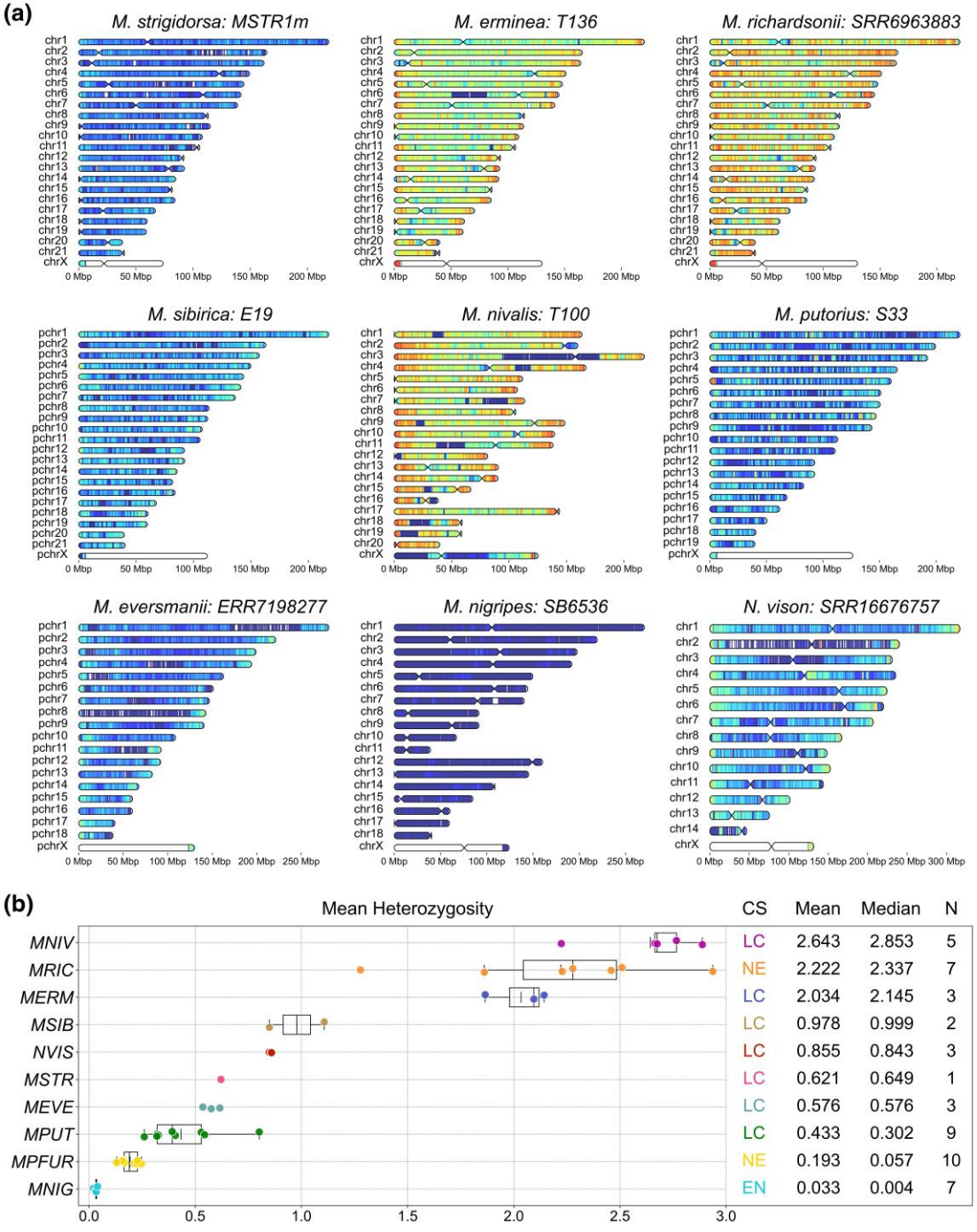

Fig. 5. Heterozygosity of Mustelinae species. a) Distribution of the heterozygous SNP density on the chromosomes of Mustelinae species. Heterozygous SNPs were counted in 1 Mbp windows with 100 kbp steps and scaled to SNPs/kbp (represented by color scale on the left, ranging from dark blue (extremely low heterozygosity) to brown (very high heterozygosity), with 0 to 0.1 and over 6 heterozygous SNPs per 1 kbp, respectively. Centromeres are not indicated for pseudochromosome-level assemblies where chromosomes are labeled with the prefix "pchr." Each heatmap represents a single individual selected as a representative of the corresponding species. b) Intra and interspecific heterozygosity among Mustelinae species. The values at the top of the figure reflect the intraspecies mean and median heterozygosity. Short vertical lines within boxplots represent the mean value and long lines indicate the median value. Each dot corresponds to a separate individual. Species abbreviation: MNIG, *Mustela nigripes*; MPFUR, *Mustela putorius furo*; MPUT, *Mustela putorius*; MEVE, *Mustela eversmanii*; MSTR, *Mustela strigidorsa*; NVIS, *Neogale vison*; MSIB, *Mustela sibirica*; MERM, *Mustela erminea*; MRIC, *Mustela richardsonii*; MNIV, *Mustela nivalis*. Species global conservation status (CS) according to IUCN data: EN, endangered; NE, not evaluated; LC, least concern; *N*, number of individuals. Detailed data are provided in Table S9. Distribution of heterozygous SNP density on chromosomes for the other samples is presented in the Supplementary File.

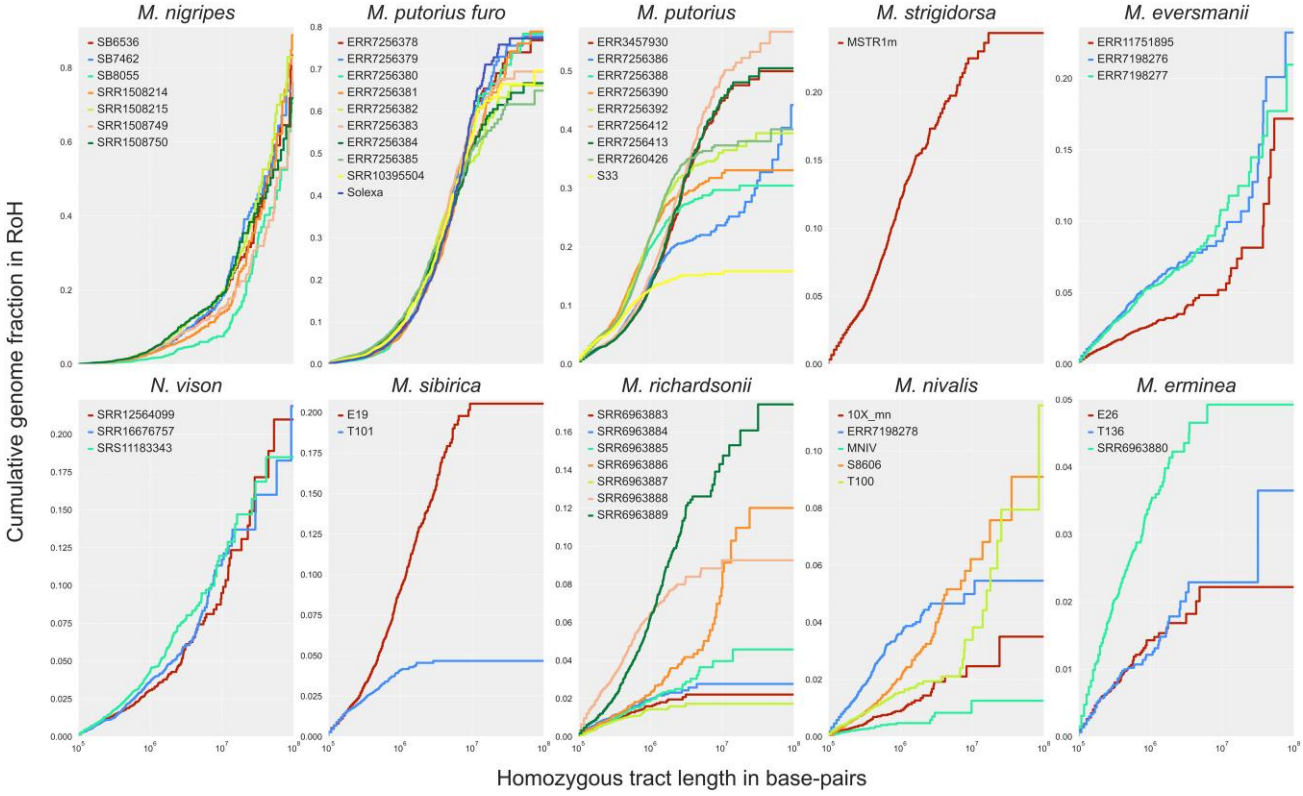

Fig. 6. The runs of homozygosity (RoH) content in the Mustelinae samples by species. Cumulative distribution plots of RoH. Homozygous tract lengths and cumulative genome fraction in RoH are represented on *X* and *Y* axes. Tracts are ordered from shortest to longest. *X* chromosomes were excluded from all samples. Detailed data are provided in Fig. S10 and Table S10.

differences: *M. putorius* (0.26–0.8), *M. eversmanii* (0.54–0.62), *M. sibirica* (0.85–1.11), *M. richardsonii* (1.28–2.94), *M. erminea* (1.87–2.14), and *M. nivalis* (2.23–2.9). Species with restricted distributions or a domestication history had uniformly low diversity (*M. nigripes* 0.02–0.04, *M. putorius furo* 0.13–0.25, *N. vison* 0.85–0.86). *M. strigidorsa* is represented by a single sample with mean heterozygosity of 0.62 SNP/kbp.

Extensive homozygosity is evident in *M. nigripes* and *M. putorius furo* (Fig. 6, Fig. S10, Table S10): *M. nigripes* RoH cover 2.1–2.2 Gbp (86.83% to 91.66%) out of 2.5 Gbp of the genome assembly with 77.83% to 91.81% in ultra-long tracts (≥10 Mbp), while *M. putorius furo* had a 1.48–1.88 Gbp fraction (64.9% to 82.05%) of the genome assembly, of which 38.75% to 54.09% were long RoH (≥1 Mbp). *M. putorius* has the highest variation in total RoH length (371.8 Mbp–1.4 Gbp; 15.84% to 59.28%): RoH in European mainland individuals encompass from 15.84% to 39.96% of the genome assembly (2.5 Gbp) and most are short (<1 Mbp), whereas UK samples have a RoH fraction 49.87% to 52.75% of the genome assembly. Sample ERR7256386 (Spain) stands out from the other samples by its RoH content (1.4 Gbp in total), with a major contribution from ultra-long RoH (60.1%). In *M. eversmanii* samples 335–631 RoH accounted for 23.47% to 27.84% of the genome assembly, with 57.35% to 77.9% contained in 9–13 ultra-long tracts. Highly heterozygous species (*M. richardsonii*, *M. erminea*, *M. nivalis*) were largely devoid of RoH, aside from isolated long segments. For example, *M. nivalis* T100 had 270 Mbp (11.6%) and S8606 131 Mbp (5.63%), with T100 including seven ultra-long RoH up to 85 Mbp.

PSMC trajectories were consistent with these diversity patterns. High-diversity species showed large and relatively stable historical N_e (Fig. 7). European *M. nivalis* samples displayed a steady N_e increase following divergence from Asian lineages 1 Mya (Mid-Pleistocene Transition (MPT), confidence interval (CI): from 629.6 kya to 1.6 Mya), reaching up to 62.6k. Asian individuals remained lower (up to 20.4k) and did not show recovery. *M. erminea* exhibited parallel trajectories across samples, with N_e rising until 100 kya (CI: 63–157.8 kya, max 22.7–25.1k) before a gradual decline. *M. richardsonii* and *M. erminea* diverged 2 Mya (CI: 1.3–3.2 Mya), followed by elevated N_e (max 17.5–22.6k) and stabilization near 200 kya (CI: 125.9–315.6 kya). The hybrid

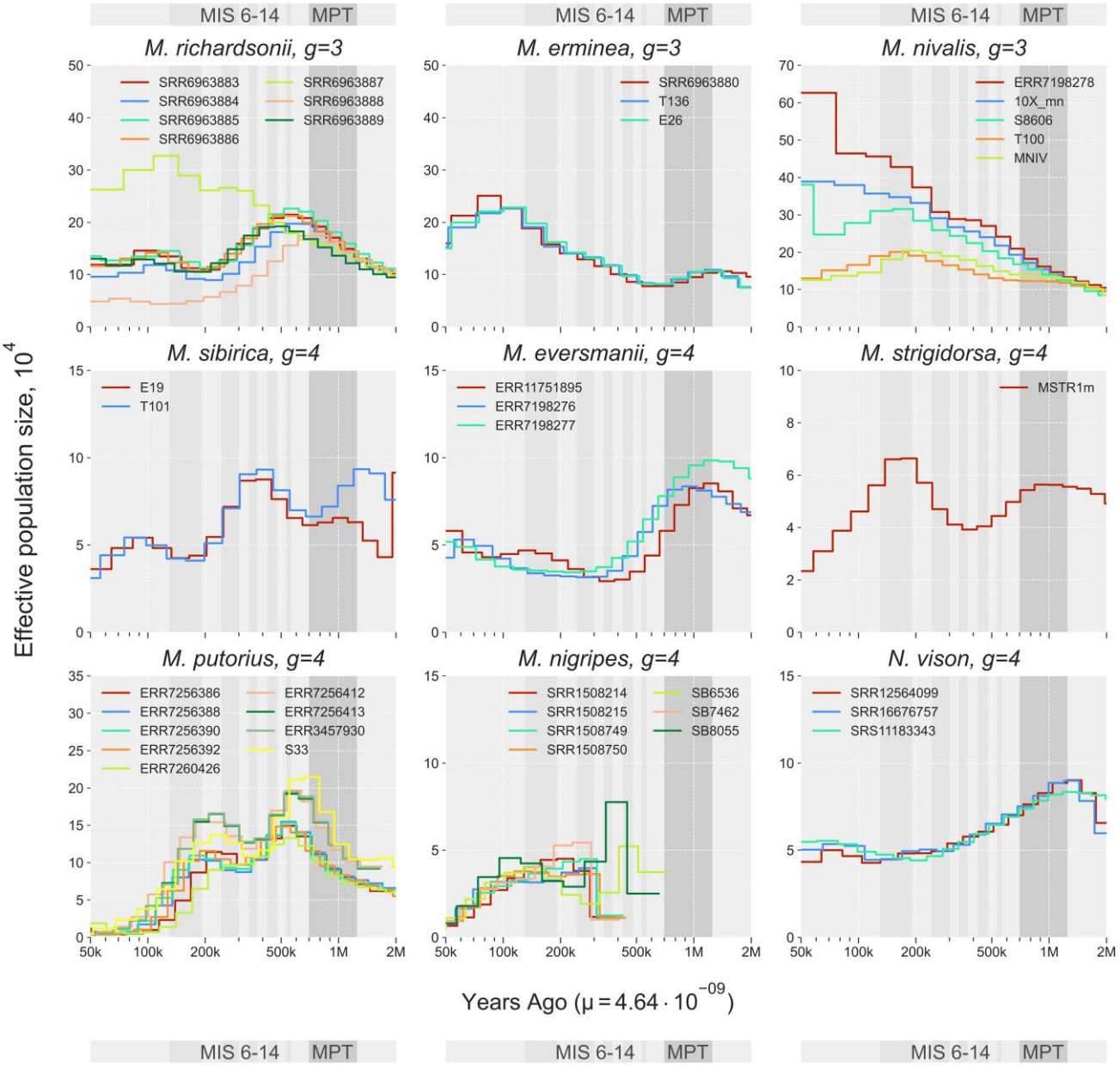

Fig. 7. Demographic history of Mustelinae species. The *X* chromosome was excluded from the analysis. Parameters: g, generation time, μ, mutation rate. Abbreviations: MIS, Marine Isotope Stages: 6 (191–130 kya), 7 (243–191 kya), 8 (300–243 kya), 9 (337–300 kya), 10 (374–337 kya), 11 (424–374 kya), 12 (478–424 kya), 13 (533–478 kya), 14 (563–533 kya); MPT, Mid-Pleistocene Transition (1.25–0.7 Mya).

M. richardsonii × *M. erminea* individual (SRR6963887) (Colella et al. 2018, 2021) showed a distinct continuous increase to 32.7k until 150 kya (CI: 94.4–236.7 kya). Species with lower heterozygosity and extensive RoH experienced recurrent or prolonged bottlenecks. *M. sibirica* showed two contractions (at 350 kya, CI: 220.4–552.4 kya; and at 100 kya), reducing N_e from 8.8k to 4.1k. *M. eversmanii* underwent a sharp decline beginning 1 Mya, reaching minima of 2.9–3.4k. *M. strigidorsa* exhibited two reductions (850 kya, CI: 535.1 kya–1.3 Mya, to 350 kya; and 150 kya) to a minimum of 2.3k. *M. putorius* experienced two pronounced bottlenecks (500 kya, CI: 314.8–789.1 kya; and 200 kya), reducing N_e to 0.4–1.2k; continental and UK individuals formed two clusters but shared the same decline pattern. In *M. nigripes*, extremely low genomic diversity restricted inference to 350 kya, with consistently low N_e (0.7–1.1k). All *N. vison* samples showed a prolonged decline beginning 1 Mya, stabilizing around 300 kya (CI: 188.9–473.5 kya).

Discussion

Genome Assembly Length vs. Genome Size

In recent years, chromosome-level genome assemblies have become the gold standard in comparative and population genomics, providing highly detailed genomic structures and facilitating sophisticated genetic studies (Theissinger et al. 2023). Within the Mustelinae, however, such resources remain scarce (Table S1): only six chromosome-level and two scaffold-level assemblies were previously available, with considerable variability in assembly quality due to differences in sequencing technologies. Long-read–based assemblies of *M. erminea*, *M. lutreola* and *N. vison* stand out for high continuity and BUSCO completeness, whereas our new chromosome-level assemblies of *M. nivalis* and *M. strigidorsa* as well as the scaffold-level assembly of *M. sibirica* achieve quality metrics comparable to those of other *Mustela* genomes (Tables S4 and S6). Despite this progress, genome assemblies for 11 Mustelinae species are still missing, largely due to difficulties in obtaining samples from tropical regions (*M. kathiah*, *M. nudipes*, *M. lutreolina*) and from geographically restricted islands (*M. haidarum*, *M. itatsi*). The newly generated *M. strigidorsa* genome assembly broadens taxonomic representation within tropical Asian Mustelinae and provides a critical reference for future comparative and phylogenomic studies.

According to previous cytogenetic studies, Mustelinae species are often characterized by completely heterochromatic arms (consisting almost exclusively of the additional heterochromatin) on originally acrocentric chromosomes (Graphodatsky et al. 1977, 1989). Depending on lengths, which vary from species to species, they can notably affect the genome sizes (Graphodatsky et al. 1977). These heterochromatin blocks, comprised largely of difficult-to-sequence tandem repeats with high GC content, are often poorly represented in assemblies due to sequencing biases and the discarding of repeat-associated reads during assembly (Biscotti et al. 2015; Sedlazeck et al. 2018). Our data appear to confirm that differences in heterochromatin content underlie the variability in genome size among Mustelinae species, as indicated by discrepancies between estimates derived from genome assemblies and 23-mer distribution of WGS reads (Fig. 2, Table S5). These discrepancies are evident when comparing genome size estimates from different methods, such as k-mer distribution analysis of WGS data (Kliver et al. 2017; Ranallo-Benavidez et al. 2020) and cytogenetic analysis (Hardie et al. 2002). Cytogenetic data suggest the euchromatic portion remains stable across Mustelidae species (2.4 to 2.9 Gbp, which corresponds to 2.5 to 3 pg [Doležel et al. 2003]) (Graphodatsky 1989), with size differences attributed to heterochromatin variation (Graphodatsky et al. 1977). In our study, genome assemblies (2.41–2.68 Gbp, Table S4) and 23-mer WGS-based estimates (Table S5) consistently yielded smaller sizes than cytogenetic measurements. Species with minimal heterochromatin content such as *M. sibirica* (13.4% ± 4.7% [Graphodatsky et al. 1977]) with an assembly length of 2.4 Gbp showed moderate differences in genome size (cytogenetic: 3.0–3.1 Gbp = 3.1 to 3.2 pg vs. WGS: ~2.54–2.59 Gbp), while those with substantial heterochromatin like *M. nivalis* (34.5% ± 3.2% heterochromatin [Graphodatsky et al. 1977]) with an assembly length of 2.45 Gbp exhibited more dramatic disparities (cytogenetic: 4.4 Gbp = 4.5pg vs. WGS: 3.08–3.35 Gbp). In other Mustelinae species, such as *M. eversmanii*, *M. putorius*, *M. erminea* and *N. vison*, the heterochromatin content is 20.6% ± 2.2%, 22.7% ± 3.4%, 22.8% ± 3.5% and 25.4% ± 4.7%, respectively (Graphodatsky et al. 1977). These inconsistencies likely stem from incomplete assembly of heterochromatic regions in genome sequencing approaches, compounded by the high error margins (up to 15%) in heterochromatin quantification methods (Graphodatsky et al. 1983; Graphodatsky 1989).

Phylogeny and Ancestral Rearrangements

Previous Mustelinae phylogenies were primarily based on concatenated mitochondrial and/or limited nuclear markers (Koepfli et al. 2008a; Sato et al. 2012; Law et al. 2018; Hassanin et al. 2021). We performed such a reconstruction using whole-genome data for the first time, including new genome assembly and resequencing data of two Asian species, *M. strigidorsa* and *M. sibirica* (Fig. 4a). *M. strigidorsa*, which is distributed in the tropical regions of Southeast Asia, occupied a basal position relative to other *Mustela* species in the phylogenetic trees (Fig. 4a, Figs. S5 and S6). For three more tropical Asian species (*M. kathiah*, *M. nudipes,* and *M. lutreolina*), whole-genome data are still unavailable, but mitochondrial genome reconstructions suggest successive splitting of *M. nudipes* and *M. kathiah* from the stem (Hassanin et al. 2021), while concatenated nuclear + mitochondrial DNA datasets group *M. nudipes* with *M. strigidorsa* together as sister taxa (Koepfli et al. 2008a; Sato et al. 2012; Law et al. 2018). However, mtDNA trees might be unreliable in case of mustelids, due to active interspecies hybridization within this family, which was reported for multiple species: badgers, martens, ermines, ferrets and others (Rozhnov et al. 2013; Kinoshita et al. 2019; Colella et al. 2021; Szatmári et al. 2021; Etherington et al. 2022; Tomarovsky et al. 2025). Breeding in captivity has also revealed that distantly related species such as *M.*

putorius and *M. sibirica* are capable of hybridizing (Graphodatsky et al. 1982, 1985). In our study we observed some discordance between nuclear (Fig. 4a) and mitochondrial (Fig. S8) trees. For example, the *M. putorius* ERR7260426 (BK069848) sample was previously shown to have such a discordance (Etherington et al. 2022); inclusion of all available genome data from the Mustelinae clarified that this sample carries a *M. lutreola* mitochondrial genome.

Our species tree (Figs. S5 and S6) supports the distinction between *N. vison* and the genus *Mustela*, with high main posterior probability support (pp1 = 1.0, Table S8). While quartet support for this split was somewhat lower than for other interspecific nodes (q1 = 61.7%), it remains above the threshold typically considered indicative of primary topological signal. This moderate value may reflect inherent gene tree discordance due to incomplete lineage sorting or ancient gene flow at the early stages of Mustelinae diversification. Nonetheless, both concatenated (Fig. 4a) and coalescent-based (Figs. S5 and S6) analyses consistently recover *N. vison* as a sister lineage to *Mustela*, supporting the current taxonomic treatment that recognizes *Neogale* as a distinct genus. While most interspecific nodes were characterized by high quartet support, a notable exception is node 9, uniting *M. sibirica* and *M. lutreola*, which showed markedly reduced support (q1 = 47.7%, Table S8), likely reflecting conflicting gene tree signals in this part of the phylogeny. At the same time, the position of *M. strigidorsa* as the earliest branching lineage within *Mustela* is strongly supported, further reinforcing its placement within this genus.

M. erminea sensu *lato* (all stoats) and *M. nivalis* are the Mustelinae species with the largest ranges, encompassing nearly the whole Holarctic (Fig. 1). The combination of such a wide distribution and limited dispersal due to small body sizes suggested to researchers that these two taxa might contain multiple species. Recently, *M. erminea* sensu *lato* was split into three species: *M. erminea (*sensu stricto, Eurasia and Alaska), *M. richardsonii* (continental America), and *M. haidarum* (Haida Gwaii and Alexander Archipelago of coastal North America) (Colella et al. 2021). However, this suggestion was based on mitochondrial sequences and morphological traits only. By combining samples from a previous dataset (Colella et al. 2018) and sequencing two more *M. erminea* individuals from Yakutia, Russia, we confirmed the hypothesis of multiple species (Supplementary Results, Discussion, and Methods). Due to the lack of samples, the status of European *M. erminea* remains unclear. For *M. nivalis* we found that despite clear division of Western European and Asian samples, pairwise distances between them are comparable to distances within *M. erminea* (Fig. 4b, Fig. S9), i.e. no signs of speciation were observed. However, it is important to note that within-species divergence was assessed for Eurasian *M. nivalis* only, due to the lack of samples from North America.

The order Carnivora was suggested to have an ancestral karyotype with 2*n* = 38 (Nash et al. 2008; Perelman et al. 2012; Beklemisheva et al. 2016), which is observed across a wide range of terrestrial and semiaquatic species (Graphodatsky et al. 2020). Within Carnivora, the Mustelidae also exhibits a predominantly syntenic conservatism with 2*n* = 38 in most species (Graphodatsky et al. 2020). However, several lineages within Mustelidae show notable variation in chromosome number, for example, Melinae (e.g. *Meles*, 2*n* = 44) and Guloninae (e.g. *Martes*, 2*n* = 38–40; *Gulo*, 2*n* = 42), reflecting independent chromosomal rearrangements (Graphodatsky et al. 2020). One such example is the Mustelinae, which displays considerable karyotypic variability (Figs. 3 and 4a). Within this group, the diploid number ranges from 2*n* = 30 in *N. vison* to 2*n* = 44 in species such as *M. strigidorsa*, *M. kathiah* (Abramov et al. 2013), *M. erminea,* and *M. altaica* (Graphodatsky et al. 2020). This variability likely reflects a history of recurrent chromosomal fissions and fusions, which have contributed significantly to the evolutionary diversification of the subfamily. The results of our study allow us to clarify the timing of the three latest chromosomal fissions in Mustelinae (Fig. 4c). All three rearrangements occurred after the divergence of Mustelinae from other Mustelidae lineages and at early stages of the subfamily's radiation (Fig. S7). These events were previously identified (Graphodatsky et al. 2002), but two of them are now confirmed to have taken place before the diversification of extant Mustelinae, while the timing of the third fission has been revised based on our data. Earlier hypotheses suggested that the fission fis(MSTR2, MSTR21) occurred after the divergence of the *Neogale* lineage but before the separation of *M. erminea* (Graphodatsky et al. 2002). The inclusion of *M. strigidorsa* in our phylogenetic analysis provides important new evidence. This species occupies a basal position within the *Mustela* clade (Fig. 4a), which shifts the previously proposed timing of the fission event. Additional support for the ancestral Mustelinae rearrangements comes from data on other tropical *Mustela* species. For example, *M. kathiah* has been shown in previous studies (Sato et al. 2012; Law et al. 2018), as well as in our mitochondrial genome analysis (Fig. S8), to have diverged after *M. strigidorsa*. Furthermore, *M. nudipes* is phylogenetically close to *M. strigidorsa* (Koepfli et al. 2008a; Sato et al. 2012; Law et al. 2018), and *M. lutreolina* is another tropical species potentially related to this group. However, the phylogenetic position of *M. lutreolina* remains uncertain, as no cytogenetic or genomic

data are currently available for this species. These observations support the inference that the ancestral *Mustela* karyotype most likely had a diploid number of $2n = 42$ (Fig. 4c). The ancestral karyotype of the genus *Neogale* remains uncertain. In *N. vison*, several chromosomal fusions have been identified, resulting in a reduced chromosome number of $2n = 30$ (Fig. 3). However, it is not yet clear whether these chromosomal rearrangements are specific to this species or represent a broader pattern shared across the genus. Further studies, including data from other *Neogale* species are necessary to address this question.

Genetic Diversity and Demographic Histories

Maintaining genome-wide genetic variation is widely considered critical for population viability (Lande and Shannon 1996; Abascal et al. 2016; Bozzuto et al. 2019), while some argue for focusing on functionally important variation (Robinson et al. 2016, 2019; Teixeira and Huber 2021). Despite ongoing debates, there is broad consensus that reduced genome-wide diversity can affect long-term viability, despite context-dependent effects. Mustelinae species, like others, are subject to varying climatic and ecological pressures, leading to significant fluctuations in their genetic diversity (Colella et al. 2018; de Ferran et al. 2022; Derežanin et al. 2022). In our study, we evaluated genetic diversity by assessing and comparing genome-wide heterozygosity and homozygosity within and between species (Figs. 5 and 6), as well as investigating their distribution within the genomes. In addition, our demographic analysis revealed significant variation in effective population size among *Mustela* species (Fig. 7), reflecting biogeographic history and responses to Pleistocene climate change. Although our data do not cover population-level resolution, they provide an initial genome-wide overview and demonstrate shared impacts of large-scale environmental factors.

We found considerable intraspecific and interspecific differences in mean heterozygosity between analyzed *Mustela* species (Table S9): from 0.02 SNPs/kbp to 2.9 SNPs/kbp. The most heterozygous species included the widely distributed *M. nivalis* (2.64 SNP/kbp), *M. erminea* (2.03 SNP/kbp) and *M. richardsonii* (2.22 SNP/kbp). The observed high genetic diversity in *M. nivalis* samples aligns with previous studies based on different molecular markers, including mitochondrial sequences (Lebarbenchon et al. 2010; Sato et al. 2020; Tissaoui et al. 2024). However, despite the high mean heterozygosity of this species, we observed clear signs of recent inbreeding, indicated by the presence of ultra-long RoH (e.g. in sample T100, Table S10) covering significant portions of their chromosomes. This is consistent with monitoring studies that show declines in local populations of *M. nivalis* in regions such as the USA (Jachowski et al. 2021), UK (Sainsbury et al. 2019), Spain (Llorca et al. 2024) and Tunisia (Hayder et al. 2023).

A combination of high heterozygosity and broad ecological tolerance in *M. nivalis* and *M. erminea* (Sommer and Crees 2022) likely promoted their demographic stability during climatic oscillations. Both show either continuous growth or consistently elevated N_e during MIS (Marine Isotope Stage) 14–6 (Fig. 7), a period of strong climatic instability. These patterns are consistent with their persistence across glacial–interglacial cycles and broad geographic ranges (Sommer and Benecke 2004; Sommer and Crees 2022), a notion further supported by fossil evidence (Sommer and Benecke 2004; Marciszak and Socha 2014; Krajcarz et al. 2015; Kosintsev et al. 2016; Crégut-Bonnoure et al. 2018; Giustini et al. 2024). A more detailed look reveals a structured demographic history for *M. nivalis*, with western (European) and eastern (Asian) lineages diverging around 1 Mya during the MPT, followed by sustained N_e growth in the west and relative stability in the east. We hypothesize that the elevated N_e in Europe may indicate historical gene flow, a pattern similar to that observed in the hybrid *M. richardsonii* × *M. erminea* individual (SRR6963887), where introgressive hybridization is well documented (Colella et al. 2018). Such complex introgression signatures, also observed in other Mustelidae hybrids like *M. zibellina* × *M. martes* (Tomarovsky et al. 2025), can be indirectly detected by PSMC, which, while not explicitly inferring admixture, offers indirect evidence of complex histories. The demographic stability in eastern *M. nivalis* also has a broad range overlapping. distributed taxon but has been relatively understudied. Its intraspecific structure remains unknown and the species is still treated as a single taxonomic unit. Consequently, there is reason to suggest that *M. nivalis* may comprise distinct, geographically structured lineages that could warrant species-level recognition consistent with a possible Asian origin and later westward expansion. *M. erminea* shows a broadly similar trajectory, with N_e increase during MIS 14–6 followed by decline near the end of MIS 6. However, due to sampling from eastern populations only, spatial inferences are limited. Nevertheless, the concordant demographic patterns observed in *M. nivalis* and *M. erminea* support the hypothesis that their persistence was shaped by shared ecological mechanisms, particularly their high adaptability to cold climates during periods of Quaternary climatic instability.

In stark contrast to these widespread species, we observed significantly lower heterozygosity and extensive RoH in the less widespread *Mustela* species (Tables S9

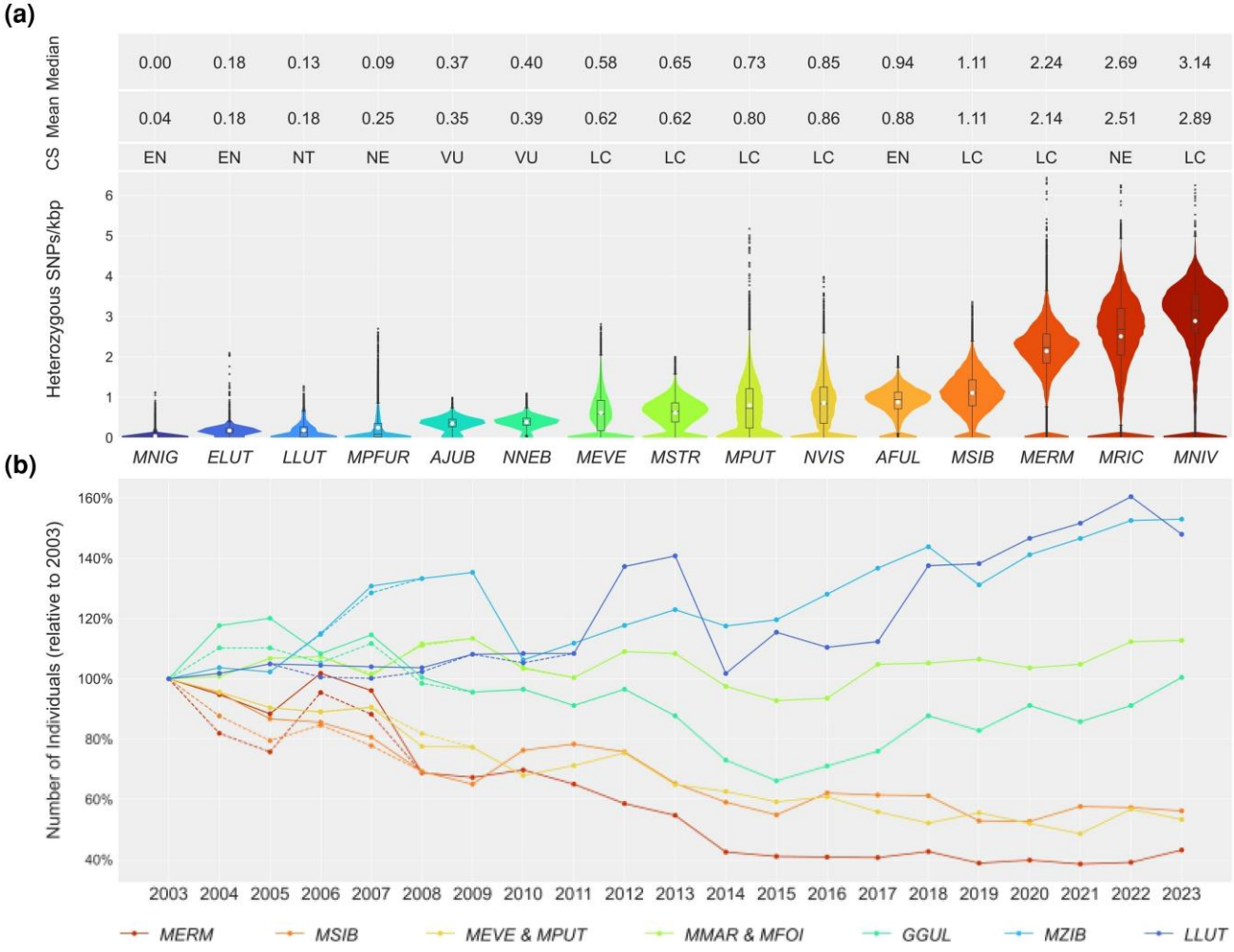

Fig. 8. Distribution of the heterozygous SNP density in Mustelinae species and five well-known in conservation genetics species: *Enhydra lutris*, *Lutra*, *Acinonyx jubatus*, *Neofelis nebulosa*, and *Ailurus fulgens* (Totikov et al. 2021), and the status of main fur game species in Russia. a) Heterozygous SNPs were counted in 1 Mbp windows and 100 kbp steps and scaled SNPs/kbp for all species. Only samples with highest mean values are shown (one sample per species, Table S9). Median and mean heterozygosity values are indicated within boxplots by black line and white dots, respectively. Color gradient indicates the level of heterozygosity, ranging from lower (blue) to higher (red) values. b) The main fur game animal resources in the Russian Federation for the years 2003 to 2023. Data are based on public reports of the Ministry of Natural Resources and Environment of the Russian Federation and the Federal Research Center for Hunting Development (Lomanov et al. 2007; Minprirody of Russia 2024). Dotted lines indicate discrepancies in the datasets (Table S11). Abbreviations: GS, Global conservation status according to IUCN Red List data; LC, Least Concern; NT, Near Threatened; VU, Vulnerable; EN, Endangered; NE, not evaluated; Species: MNIG, *Mustela nigripes*; ELUT, *Enhydra lutris*; LLUT, *Lutra*; MPFUR, *Mustela putorius furo*; AJUB, *Acinonyx jubatus*; NNEB, *Neofelis nebulosa*; MEVE, *Mustela eversmanii*; MSTR, *Mustela strigidorsa*; MPUT, *Mustela putorius*; NVIS, *Neogale vison*; AFUL, *Ailurus fulgens*; MSIB, *Mustela sibirica*; MERM, *Mustela erminea*; MRIC, *Mustela richardsonii*; MNIV, *Mustela nivalis*; MMAR, *Martes*; MFOI, *Martes foina*; GGUL, *Gulo*; MZIB, *Martes zibellina*.

and S10), which is consistent with evidence of recurrent or prolonged bottlenecks (Fig. 7). A notable example is the tropical *M. strigidorsa*, the species previously unassessed on the genome level. The single sample from Vietnam has a mean heterozygosity of only 0.62 SNP/kbp (Fig. 8a), with RoH covering 23.62% of its genome. While it exhibits relatively moderate homozygosity, its genome shows both long (10.21%) and ultra-long (1.81%) RoH. Although there are concerns regarding habitat degradation and fragmentation for this species, their effect on its population size remains unknown due to limited data (Abramov et al. 2008). Its genetic diversity is significantly lower than that of another South Asian species with endangered status, *Ailurus fulgens* (Fig. 8a). Furthermore, similarly with *M. eversmanii*, it occupies an intermediate position between the highly heterozygous Mustelinae and species with well-documented threatened status, including

Enhydra lutris, *Lutra lutra*, *Acinonyx jubatus*, and *Neofelis nebulosa* (Fig. 8a). At the extreme end of the homozygosity spectrum is *M. nigripes*, a species once declared extinct (Fricke 2015), where RoH cover at least 87% of the genome, and heterozygosity ranges from 0.02 to 0.04 SNP/kbp (Derežanin et al. 2025)—significantly lower than that of the domesticated *M. putorius furo*.

The pattern of low diversity extends to *M. eversmanii* (Fig. 5), represented in our study by three samples from its Asian range, which exhibit relatively low mean heterozygosities (0.54, 0.58, and 0.62 SNPs/kbp). This species is considered to be rapidly disappearing in several European countries (Šálek et al. 2013), facing severe threats including habitat loss and fragmentation, declining prey base, competition, and rodenticide poisoning (Šálek et al. 2013; Szapu et al. 2024). Conversely, a recent study based on low-resolution data challenges the alarming rate of decline in Europe, suggesting either insufficient research or a rapid population recovery following a sharp decline (Szatmári et al. 2021). Assessments in its Asian range are scarce, but reports indicate a significant decline in Russia (Lomanov et al. 2007; Kiseleva 2024; Minprirody of Russia 2024). There, the combined population estimate of *M. eversmanii* and *M. putorius* (due to nearly indistinguishable tracks) dropped from 90.6 to 48.3k individuals between 2003 and 2023 (Fig. 8b, Table S11), with two species believed to contribute approximately equally to these counts (Lomanov et al. 2007; Minprirody of Russia 2024). Although the causes of *M. eversmanii* decline in Russia remain unclear, current evidence suggests contributions from competition with the invasive *N. vison* (Macdonald and Harrington 2003; Croose et al. 2018; Kiseleva 2024), long-term declines of its key prey *Spermophilus erythrogenys* due to extensive control programs (Shilova 2011; Vazhov et al. 2016; Wright et al. 2022), and broader threats across its range, while habitat loss and hunting pressure appear minor (detailed data are provided in Supplementary Results, Discussion, and Methods) (Kiseleva 2024). A similar situation is observed in *M. putorius*, which also shows low genetic diversity (0.43 SNPs/kbp) and high RoH (15.84% to 59.28%). Populations are declining in Europe due to factors overlapping with *M. eversmanii*, such as competition with invasive predators (Croose et al. 2018). Notably, while hybridization with *M. putorius furo* has contributed to population recovery in the UK (Shaw et al. 2025), increasing competition with *N. vison* remains a threat (Croose et al. 2018).

Unsurprisingly, given their low genetic diversity and current threats, the demographic histories of these less widespread species show evidence of recurrent or prolonged bottlenecks. *M. putorius*, widespread in Europe, experienced two sharp N_e declines during MIS 12 and MIS 6 (Fig. 7). Despite this, it is considered an early post-LGM (Last Glacial Maximum) recolonizer of Central Europe, supported by fossil data (Sommer and Benecke 2004; Sommer and Crees 2022). Other species, sampled from Asia, show bottlenecks around the onset of the 100-kyr glacial cycles. Although Asia is thought to have been less impacted by Quaternary climate shifts (Fu and Wen 2023), our results suggest substantial demographic changes even in steppe and tropical-adapted species. Fossil data for these taxa remain limited (Krajcarz et al. 2015; Kosintsev et al. 2016; Giustini et al. 2024; Fourvel et al. 2025): *M. eversmanii* is known from seven European Pleistocene sites (including *M. stromeri*, its common ancestor with *M. putorius* and *M. nigripes*); *M. sibirica* from two Japanese finds; and *M. strigidorsa* lacks confirmed Pleistocene records (Peters and McClennen 2016). Southern Polish (Krajcarz et al. 2015) and Ural (Kosintsev et al. 2016) fossils suggest a broader range for *M. eversmanii* during the Pleistocene, later restricted to Eastern European steppes.

Overall, *Mustela* demographic histories highlight how long-term population dynamics reflect the interplay of environmental change and climatic history. Future studies incorporating broader genomic sampling, paleodistribution models, and molecular dating are crucial to provide a more comprehensive overview.

Conclusions and Perspectives

This study presents the first comprehensive whole-genome analysis of the subfamily Mustelinae, in which we examined chromosome-scale structural rearrangements, reconstructed phylogenetic relationships, assessed genome-wide genetic diversity, and inferred demographic history for 10 species. Our results show that genetic variability within Mustelinae is shaped by multiple demographic and ecological processes rather than by uniform evolutionary pressures. The pronounced interspecific and intraspecific heterogeneity in heterozygosity highlights the complex evolutionary dynamics operating within this group. Particular attention is drawn to *M. eversmanii* and *M. putorius*. Both species show low levels of genetic diversity, RoH tracks, and genomic signals of historical N_e reductions. For *M. eversmanii*, these patterns are evident across both the European and Asian parts of its range, suggesting that the species may be more sensitive to environmental and anthropogenic pressures than previously assumed. Similar genomic signals in *M. putorius* raise concerns that its current classification as Least Concern may not completely capture its real conservation status. Although our results do not, by themselves, justify IUCN Red List reclassification, they indicate that a

more detailed evaluation of genetic and demographic trends would be valuable for refining conservation priorities. Overall, the findings emphasize the need for regular monitoring of genetic diversity in *Mustela* species, especially in taxa with ongoing population declines and potentially reduced efficacy of purifying selection.

Our phylogenomic reconstruction, the first based on whole-genome data for Mustelinae, refines the evolutionary relationships within the subfamily and supports several key taxonomic conclusions. The results confirm the validity of the genus *Neogale*, support the placement of *M. strigidorsa* within the genus *Mustela*, and validate the species status of *M. richardsonii*. Nuclear and mitochondrial datasets produced largely congruent topologies, but several discrepancies were detected, likely caused by interspecific hybridization. The first genome of *M. strigidorsa*, the representative of the tropical and basal *Mustela* species, allowed us to reconstruct the earlier steps of the Mustelinae karyotype evolution and date the major chromosomal fusions and fissions. We confirmed the previously suggested hypothesis of an ancestral karyotype of $2n = 44$ for *Mustela* and $2n = 42$ for Mustelinae. However, the chromosomal evolution within the tropical lineage remains mysterious and represents a promising direction for future research.

Despite the substantial amount of new genomic information generated in this study, many questions remain open, largely because biological samples are difficult to obtain for species with limited or hard-to-access ranges. Future research will benefit from expanding geographic sampling, including unsequenced species, and integrating additional population-level data. Such efforts will allow a more complete understanding of genetic structure, refine models of chromosomal evolution, and support evidence-based strategies for the long-term conservation of mustelid biodiversity.

Materials and Methods

Samples, DNA Extraction and Sequencing

To generate data for the chromosome-level genome assemblies, we used a primary fibroblast cell lines from male *M. strigidorsa* (MSTR1m, AVA 19-021, origin: Quang Nam, Vietnam) and from male *M. nivalis* (MNIV1m, origin: Novosibirsk, Russia). The cell lines were provided by the large-scale research facilities "Cryobank of cell cultures," Institute of Molecular and Cellular Biology SB RAS. We used frozen muscle tissue from a male *M. sibirica* (MSIB1m, origin: Sakha Republic, Russia) to generate a scaffold-level genome assembly. For whole-genome resequencing of *M. nivalis*, *M. erminea*, *M. sibirica,* and *M. putorius*, we used both muscle tissue and primary fibroblast cell lines. The resulting dataset, combined with publicly available data, consisted of 50 whole-genome samples representing 10 species from the Mustelinae. A detailed description of the resequencing data is provided in Table S12 and includes both previously published and new data generated within our study.

DNA extraction was performed using the standard phenol–chloroform protocol (Sambrook and Russell 2006). The extracted DNA was fragmented using a Covaris instrument to reach the desired insert size and libraries were constructed with the TruSeq DNA PCR-Free kit (Illumina, Inc., San Diego, CA, USA). For the chromosome-level genome assemblies, we generated Hi-C libraries following the original protocol (Rao et al. 2014). All prepared libraries were sequenced with paired-end 150 bp reads on the Illumina NovaSeq 6000 platform. An Oxford Nanopore Technologies library was also prepared for the *M. strigidorsa* sample using the SQK-ULK114 kit and sequenced on a 10.4.1 PromethION flow cell with triple loading.

Assembly of the *M. Strigidorsa*, *M. Nivalis*, and *M. Sibirica* Genomes

We assembled the *M. strigidorsa* genome using Oxford Nanopore long reads (SRR30615031), generated as part of this study, and Hi-C (SRR34091397) and Illumina libraries (SRR34068022), generated by the DNA Zoo Consortium (Dudchenko et al. 2017). We removed adapters from the Oxford Nanopore data using Porechop v0.5.0 with ab initio adapter detection turned off, as in the test runs with the "–ab_initio" option, we detected trimming of mustelid-specific sequences present in the genome assembled using different technologies (Wick et al. 2017). Next, we filtered the data by quality (only reads with mean quality >7 were retained) and trimmed 30 bp from each end using the Chopper v0.8.0 tool (De Coster and Rademakers 2023). First, an initial draft assembly was generated from a single paired PCR-free Illumina library using w2rap-contigger (Clavijo et al. 2017), see (Dudchenko et al. 2018) for details. On the second step, the generated assembly was scaffolded using the SAMBA (script *samba.sh* with "-m 2500" option) tool (Zimin and Salzberg 2022) from MaSuRCA package v 4.1.0 (Zimin et al. 2013) and the filtered Nanopore data. Errors introduced by the long reads were corrected using the POLCA (from the same version of MaSuRCA) polisher (Zimin and Salzberg 2020) and the Illumina data. Next, we aligned the Hi-C data to the corrected intermediate assembly using Juicer v1.6 (Durand et al. 2016), followed by scaffolding to chromosome-level using 3D-DNA pipeline v210623 (Dudchenko et al. 2017) with subsequent manual

curation in Juicebox v2.16.00 (Dudchenko et al. 2018). Finally, we closed gaps using the SAMBA script *close_scaffold_gaps.sh* (with option "-m 2500") and the Oxford Nanopore reads and performed a second and third round of polishing.

We upgraded the publicly available draft genome assembly of *M. nivalis* (GCA_019141155.1), originally generated from linked-read Illumina sequencing data (Miranda et al. 2021), to chromosome-level using the Hi–C sequencing data (SRR34082581), generated by DNA Zoo Consortium. Hi–C data were aligned to the draft genome assembly using Juicer v1.6. Before alignment, the restriction sites for *Csp6I* + *MseI* were generated using *generate_site_positions.py* script in Juicer. Haplotype duplications in the alignments were identified using purge_dups v1.2.6 (Guan et al. 2020), based on sequence similarity and coverage. Regions where more than 90% of the sequence was involved in haplotype duplications were removed. Each deduplicated alignment was then processed using the 3D-DNA v210623 with the default parameters. A manual curation was performed using Juicebox v2.16.00.

To generate a draft genome assembly for *M. sibirica*, we used w2rap-contigger with the default parameters to assemble paired-end Illumina reads from sample E19. Subsequently, this assembly was scaffolded using the *M erminea* genome assembly (GCF_009829155.1) as a reference and RagTag v2.1.0 (Alonge et al. 2022) with default parameters.

Multiple Whole-genome Alignment, Synteny Blocks and Localization of Centromeres

Only the chromosomal-level genome assemblies (Table S3 in Supplementary Results, Discussion, and Methods) were used for synteny block analysis. First, we obtained a Maximum Likelihood (ML) phylogenetic tree using BuscoClade v1.7 pipeline (https://github.com/tomarovsky/BuscoClade) with default settings. Second, tandemly organized and dispersed repeats in the genome assemblies were identified and softmasked using Tandem Repeats Finder v4.09.1 (Benson 1999) with parameters "2 7 7 80 10 50 2000 -l 10", WindowMasker v1.0.0 (Morgulis et al. 2006) with default parameters, RepeatMasker v4.1.6 (Tarailo-Graovac and Chen 2009) with the parameter "-species carnivora", and BEDTools v2.31.0 (Quinlan and Hall 2010). Next, multiple WGA of all masked assemblies was performed using the obtained phylogenetic tree and Progressive Cactus v2.8.0 (Armstrong et al. 2020) with default parameters. Finally, synteny blocks were extracted from the resulting multiple alignment using halSynteny v2.2 (Krasheninnikova et al. 2020) with parameters "–minBlockSize 50000 –maxAnchorDistance 50000." The results were visualized using the script *draw_macrosynteny.py* from the MACE v1.1.32 package (https://github.com/mahajrod/MACE), with parameter "–min_len_threshold 1000000" to highlight only inversions and translocations of 1 Mbp or longer. Centromeres in the analyzed genome assemblies were localized on chromosomal scaffolds by comparison of the corresponding FISH maps and the synteny blocks. The *Canis familiaris* (UU_Cfam_GSD_1.0, [Hoeppner et al. 2014]) and *Homo sapiens* (GRCh38.p14, [Schneider et al. 2017]) genome assemblies were used as references. The detailed algorithm for identification of centromere coordinates is described in Kliver et al. (2025).

Read Filtering and Genome Size Estimation

Raw reads were trimmed from adapters and filtered by quality in various ways depending on the sequencing technology (Supplementary Results, Discussion, and Methods). Quality control of the raw and filtered reads was performed using FastQC v0.12.0 (Andrews 2010) and KrATER v2.5 (Kliver et al. 2017). Next, we counted 23-mers from the filtered reads using Jellyfish v2.3.0 (Marçais and Kingsford 2011) with the parameters "-m 23 -s 30G" for *jellyfish count* and "-l 1 -h 100000000" for *jellyfish histo*, and then visualized its distribution using KrATER with parameters "-m 23 -u 1." Finally, the genome size estimation was performed using GenomeScope v2.0 (Ranallo-Benavidez et al. 2020) in diploid mode.

Read Mapping, Variant Calling and Runs of Homozygosity

The filtered reads were first downsampled (Supplementary Results, Discussion, and Methods) to reach ~12x coverage in all samples. Next, reads from each sample were mapped to the genome assemblies corresponding to its species using BWA v0.7.17-r1188 (Li and Durbin 2009) with the default parameters. The only exception is *M. richardsonii*, for which no reference genome assembly is currently available; reads from *M. richardsonii* samples were therefore mapped to the *M. erminea* reference genome. The Samtools package v1.18 (Li et al. 2009) was then used to sort and mark duplicates in the obtained alignments. The genome coverage in the resulting alignment files was calculated using Mosdepth v0.3.3 (Pedersen and Quinlan 2018) with default parameters.

SNPs and short indels were identified using BCFtools v1.18 (Li 2011) with the following parameters: "-d 250 -q 30 -Q 30 –adjust-MQ 50 -a AD,INFO/AD,ADF,INFO/ADF,ADR,INFO/ADR,DP,SP,SCR,INFO/SCR -O u" for the *bcftools mpileup* and "–ploidy-file –samples-file –group-samples - -m -O u -v -f GQ,GP" for the *bcftools call*. The PAR coordinates (Supplementary Results, Discussion,

and Methods) were specified for variant calling via the "–ploidy-file" parameter. Low-quality genetic variants were filtered out using the *bcftools filter* with the parameters "-S. -O z –exclude "QUAL < 20.0 || (FORMAT/SP > 60.0 | FORMAT/DP < 5.0 | FORMAT/GQ < 20.0)." Based on the coverage assessments obtained from the Mosdepth analyses, individual masks for each sample were created using the *generate_mask_from_coverage_bed.py* script from the MAVR v0.97 with the parameters "-x 2.5 -n 0.33". These masks were used to remove genetic variants if coverage exceeded 250% or was less than 33% of the median genome coverage. The genetic variants were masked using the BEDTools v2.31.0 with the default parameters. The filtered and masked genetic variants for each sample were divided into heterozygous and homozygous single nucleotide polymorphisms (SNPs) and insertions/deletions (indels) using the *bcftools filter* with the parameters "-i "TYPE="snp"'", "-i "TYPE="indel"'", "-i "FMT/GT="het"'" and "-i "FMT/GT="hom"'". Heterozygous SNPs were counted in 1 Mbp windows and 100 kbp steps.

RoH were identified based on the previously calculated heterozygous SNP density in 100 kbp windows with 10 kbp steps using the *get_ROH_regions.py* script from the Biocrutch v1.0. The algorithm is detailed in (Tomarovsky et al. 2025). RoH coordinates for each sample were determined across all autosomes. The visualization of RoH on the chromosomes was performed using the *draw_features.py* script from MACE v1.1.32.

Phylogenetic Analyses

We reconstructed genome assemblies for all the resequenced samples based on the reference genome assemblies of the studied species and SNPs. Indels were not taken into account for this analysis. We used the *FastaAlternateReferenceMaker* tool from the GATK package v4.4.0.0 (Van der Auwera et al. 2013) with the parameter "–use-iupac-sample" to account for heterozygous SNPs. The obtained assemblies and the reference genome assemblies were used to identify single-copy orthologs (6,599) using BUSCO v5.6.1 with the mammalia_odb10.2024-01-08 OrthoDB v.10.1 database. To construct phylogenetic trees, we prepared two datasets: (i) a complete dataset of all resequenced samples and genome assemblies; (ii) a dataset excluding all identified hybrids (see "*Admixture analysis of stoat samples*" in Supplementary Results, Discussion, and Methods), genome assemblies, and sex chromosomes. Multiple sequence alignment was performed using MAFFT v7.490 (Kuraku et al. 2013), followed by alignment correction by the filtering of hypervariable and poorly aligned regions using Gblocks v0.91b (Castresana 2000). The multiple sequence alignment length after filtering was 11,067,417 bp. Phylogenetic trees were constructed using the ML method implemented in RAxML-NG v1.2.2 (Kozlov et al. 2024) using the GTGTR4 model and 1000 bootstrap replicates. An alternative phylogenetic reconstruction was performed using ASTRAL-III v5.7.1 (Zhang et al. 2018), based on a set of separately reconstructed gene trees using RAxML-NG. To reduce noise, we applied a filtering step by collapsing nodes with bootstrap support below 70% prior to species tree inference. The resulting phylogenetic trees were visualized using the ETE Toolkit v3.1.2 (Huerta-Cepas et al. 2016). All trees were rooted using the *Martes foina* genome assembly (mfoi.min_150.pseudohap2.1_HiC, DNA Zoo). For reproducibility of the analysis, we employed the BuscoClade v1.7. The genetic distance matrix was obtained using the Neighbor Joining (NJ) method implemented in RapidNJ v2.3.3 (Simonsen et al. 2008).

Ancestral Reconstruction of Chromosomal Rearrangements

For translocations, we created a two-state, presence (Y) or absence (N), trait matrix with species IDs as columns, and rearrangement IDs as rows. Ancestral reconstruction for the internal nodes of the inferred maximum likelihood tree from the trait matrices was performed using the continuous time Markov model implemented in the ape v5.8 package (function rerootingMethod with model="SYM") (Paradis and Schliep 2019). Depending on the predicted probabilities (PN) for "N", we classified states at internal nodes as "N" ($PN \geq 0.7$), "Y" ($PN \leq 0.3$), and "U" (unclear, $0.3 < PN < 0.7$). Our coordinate system was based on the genome assembly of *M. strigidorsa* (MSTR), which was chosen because this species occupies a basal position in the phylogenetic tree relative to all other analyzed *Mustela* species. Moreover, it provides the most convenient coordinate framework, as its chromosomes are involved only in fusion events but not in fissions relative to other species. Therefore, for each trait, we checked if the ancestral reconstruction showed "Y" for the root node. In such cases, we invert the state of the trait (from "Y" to "N" and vice versa) for both internal nodes and leaves.

Demographic History

Demographic history was reconstructed using the PSMC v0.6.5 (Li and Durbin 2011) software package with the parameters "-N25 -t15 -r5 -b -p "4 + 25 × 2 + 4 + 6'" applied to data sets both including and excluding the sex chromosomes. Genetic variants were identified using an earlier version of SAMtools v0.1.19, with the alignment quality parameter "-C 50" for *samtools mpileup* and the variant calling parameter "-c" for *bcftools view*. Diploid consensus sequences were generated

using *vcfutils.pl vcf2fq* from SAMtools, specifying the minimum ("-d") and maximum ("-D") coverage values, calculated for each sample as follows: the median genome coverage divided by 3 for the "-d" parameter and the median genome coverage multiplied by 2.5 for the "-D" parameter. Coverage values outside these ranges were filtered out. Fasta-like sequences were created using *fq2psmcfa* with a minimum nucleotide quality parameter of "-q20". Initial bootstrapping, using *splitfa*, divided the sequences into shorter segments, with 100 rounds of bootstrapping specified by the "-b" parameter for each sample. The files were prepared for visualization using *psmc_plot.pl* with "-R" parameter. Starting from values reported for the Mustelinae included in the IUCN Red List of Threatened Species (Table S1) (IUCN 2025), generation times ("-g") were slightly adjusted: 3 years were set for the relatively smaller species (*M. nivalis*, *M. erminea*, and *M. richardsonii*) and 4 years for the larger ones (*M. putorius*, *M. sibirica*, *M. strigidorsa*, *M. nigripes*, *M. eversmanii*, and *N. vison*). A mutation rate ("-u") of 4.64×10^{-9} substitutions per generation was applied, with lower (2.94×10^{-9}) and upper (7.37×10^{-9}) confidence interval derived from previous estimates of the germline mutation rate in *N. vison* (Bergeron et al. 2023).

Supplementary Material

Supplementary material is available at *Genome Biology and Evolution* online.

Acknowledgments

The unpublished genome assembly of the domestic ferret (*M. putorius furo*), Hi-C (SRR34091397) and Illumina libraries (SRR34068022) of *M. strigidorsa*, as well as Hi-C (SRR34082581) library of *M. nivalis*, were used by permission from the DNA Zoo Consortium (https://www.dnazoo.org). We acknowledge Valeriy A. Zelepukhin for helping with sample gathering. The research was completed using equipment (materials) of the large-scale research facilities "Cryobank of cell cultures" Institute of Molecular and Cellular Biology SB RAS (Novosibirsk, Russia). This research was supported in part through computational resources of HPC facilities at the collaborative center "Bioinformatics" ICG SB RAS, as well as the computing cluster of ITMO University.

Funding

Sergei Kliver was funded by the Carlsbergfondet Research Infrastructure Grant CF22-0680 and the Danish National Research Foundation award DNRF143. Alexei V. Abramov was funded by the ZIN program no.125012800908-0. José Melo-Ferreira was supported by Portuguese Fundação para a Ciência e a Tecnologia (FCT), under the ERC-Portugal programme. Inês Miranda was supported by an FCTPhD grant (SFRH/BD/143457/2019, funds from the Portuguese MCTES/FCT and ESF). Anna Zhuk was supported by St. Petersburg State University project No. 125021902561-6.

Data Availability

Genome assemblies and resequencing data are available in NCBI BioProject PRJNA1146985. Mitochondrial data obtained during the study are available at the following accession numbers: PQ246107-PQ246113, PQ821906. Mitochondrial data derived from publicly available resequencing data are available in the NCBI GenBank Third Party Annotation database under the following accession numbers: BK068807, BK068808, BK069841-BK069851.

Literature Cited

Abascal F, et al. Extreme genomic erosion after recurrent demographic bottlenecks in the highly endangered Iberian lynx. Genome Biol. 2016:17:251. https://doi.org/10.1186/s13059-016-1090-1.

Abramov A. The taxonomic status of the Japanese weasel, *Mustela itatsi* (Carnivora, Mustelidae). Zool Zhurnal. 2000:79:80–88.

Abramov AV, Duckworth JW, Wang YX, Roberton SI. The stripe-backed weasel *Mustela strigidorsa*: taxonomy, ecology, distribution and status. Mammal Rev. 2008:38:247–266. https://doi.org/10.1111/j.1365-2907.2008.00115.x.

Abramov AV, Meschersky IG, Aniskin VM, Rozhnov VV. The mountain weasel *Mustela kathiah* (Carnivora: Mustelidae): molecular and karyological data. Biol Bull. 2013:40:52–60. https://doi.org/10.1134/S1062359013010020.

Alonge M, et al. Automated assembly scaffolding using RagTag elevates a new tomato system for high-throughput genome editing. Genome Biol. 2022:23:258. https://doi.org/10.1186/s13059-022-02823-7.

Andrews S. FastQC: a quality control tool for high throughput sequence data. Babraham Bioinformatics, Babraham Institute; 2010.

Armstrong J, et al. Progressive Cactus is a multiple-genome aligner for the thousand-genome era. Nature. 2020:587:246–251. https://doi.org/10.1038/s41586-020-2871-y.

Beklemisheva VR, et al. The ancestral carnivore karyotype as substantiated by comparative chromosome painting of three pinnipeds, the Walrus, the Steller Sea Lion and the Baikal Seal (Pinnipedia, Carnivora). PLoS One. 2016:11:e0147647. https://doi.org/10.1371/journal.pone.0147647.

Belser JA, Katz JM, Tumpey TM. The ferret as a model organism to study influenza A virus infection. Dis Model Mech. 2011:4:575–579. https://doi.org/10.1242/dmm.007823.

Benson G. Tandem repeats finder: a program to analyze DNA sequences. Nucleic Acids Res. 1999:27:573–580. https://doi.org/10.1093/nar/27.2.573.

Bergeron LA, et al. Evolution of the germline mutation rate across vertebrates. Nature. 2023:615:285–291. https://doi.org/10.1038/s41586-023-05752-y.

Biscotti MA, Olmo E, Heslop-Harrison JSP. Repetitive DNA in eukaryotic genomes. Chromosome Res. 2015:23:415–420. https://doi.org/10.1007/s10577-015-9499-z.

Bozzuto C, Biebach I, Muff S, Ives AR, Keller LF. Inbreeding reduces long-term growth of *Alpine ibex* populations. Nat Ecol Evol. 2019:3:1359–1364. https://doi.org/10.1038/s41559-019-0968-1.

Cabria MT, et al. Bayesian analysis of hybridization and introgression between the endangered European mink (*Mustela lutreola*) and the polecat (*Mustela putorius*). Mol Ecol. 2011:20:1176–1190. https://doi.org/10.1111/j.1365-294X.2010.04988.x.

Castresana J. Selection of conserved blocks from multiple alignments for their use in phylogenetic analysis. Mol Biol Evol. 2000:17:540–552. https://doi.org/10.1093/oxfordjournals.molbev.a026334.

Clavijo BJ, et al. An improved assembly and annotation of the allohexaploid wheat genome identifies complete families of agronomic genes and provides genomic evidence for chromosomal translocations. Genome Res. 2017:27:885–896. https://doi.org/10.1101/gr.217117.116.

Colella JP, et al. Whole-genome analysis of *Mustela erminea* finds that pulsed hybridization impacts evolution at high latitudes. Commun Biol. 2018:1:1–10. https://doi.org/10.1038/s42003-018-0058-y.

Colella JP, Frederick LM, Talbot SL, Cook JA. Extrinsically reinforced hybrid speciation within *Holarctic ermine* (*Mustela* spp.) produces an insular endemic. Divers Distrib. 2021:27:747–762. https://doi.org/10.1111/ddi.13234.

Crégut-Bonnoure E, Boulbes N, Desclaux E, Marciszak A. New insights into the LGM and LG in Southern France (Vaucluse): the mustelids, micromammals and horses from coulet des roches. Quaternary. 2018:1:19. https://doi.org/10.3390/quat1030019.

Croose E, et al. A review of the status of the Western polecat *Mustela putorius*: a neglected and declining species? Mammalia. 2018:82:550–564. https://doi.org/10.1515/mammalia-2017-0092.

Cserkész T, et al. Intra- and interspecific morphological variation in sympatric and allopatric populations of *Mustela putorius* and *M. eversmanii* (Carnivora: Mustelidae) and detection of potential hybrids. Mammal Res. 2021:66:103–114. https://doi.org/10.1007/s13364-020-00543-6.

De Coster W, Rademakers R. NanoPack2: population-scale evaluation of long-read sequencing data. Bioinformatics. 2023:39:btad311. https://doi.org/10.1093/bioinformatics/btad311.

de Ferran V, et al. Phylogenomics of the world's otters. Curr Biol. 2022:32:3650–3658.e4. https://doi.org/10.1016/j.cub.2022.06.036.

Derežanin L, et al. Comparative analyses inform the genomic consequences of the population bottleneck in the endangered black-footed ferret. Prep. 2026.

Derežanin L, et al. Multiple types of genomic variation contribute to adaptive traits in the mustelid subfamily guloninae. Mol Ecol. 2022:31:2898–2919. https://doi.org/10.1111/mec.16443.

Doležel J, Bartoš J, Voglmayr H, Greilhuber J. Letter to the editor. Cytometry A. 2003:51A:127–128. https://doi.org/10.1002/cyto.a.10013.

Dudchenko O, et al. The Juicebox Assembly Tools module facilitates *de novo* assembly of mammalian genomes with chromosome-length scaffolds for under $1000. bioRxiv 254797. https://doi.org/10.1101/254797, 28 January 2018, preprint: not peer reviewed.

Dudchenko O, et al. De novo assembly of the *Aedes aegypti* genome using Hi-C yields chromosome-length scaffolds. Science. 2017:356:92–95. https://doi.org/10.1126/science.aal3327.

Durand NC, et al. Juicer provides a one-click system for analyzing loop-resolution Hi-C experiments. Cell Syst. 2016:3:95–98. https://doi.org/10.1016/j.cels.2016.07.002.

Etherington GJ, et al. Extensive genome introgression between domestic ferret and European polecat during population recovery in Great Britain. J Hered. 2022:113:500–515. https://doi.org/10.1093/jhered/esac038.

Fourvel J-B, Thabard C, Crégut-Bonnoure E. Fossil polecat *Mustela putorius* and *Mustela eversmanii* (Carnivora: Mustelidae) cranio-dental remains from the Pleistocene record in South-Eastern France and comments on *Mustela lutreola* skull l'Observatoire. Quat Int. 2025:739:109877. https://doi.org/10.1016/j.quaint.2025.109877.

Fricke KA. Wild again: the struggle to save the black-footed ferret by David S. Jachowski (review). Gt Plains Res. 2015:25:184–185. https://doi.org/10.1353/gpr.2015.0028.

Fu J, Wen L. Impacts of quaternary glaciation, geological history and geography on animal species history in continental East Asia: a phylogeographic review. Mol Ecol. 2023:32:4497–4514. https://doi.org/10.1111/mec.17053.

Giustini F, et al. Taxonomic and stable isotope analyses of mammal remains from the Lateglacial site of *Grotta Polesini* (central Italy): Paleoenviromental implications. J Quaternary Sci. 2024:39:1098–1115. https://doi.org/10.1002/jqs.3655.

Graphodatsky AS. Conserved and variable elements of mammalian chromosomes. In: Halnan CRE, editors. Cytogenetics of animals. CAB International Press; 1989. p. 95–124.

Graphodatsky AS, et al. Comparative molecular cytogenetic studies in the order Carnivora: mapping chromosomal rearrangements onto the phylogenetic tree. Cytogenet Cell Genet. 2002:96:137–145. https://doi.org/10.1159/000063032.

Graphodatsky AS, Isaenko AA, Radzhabli SI. Genome sizes in 28 species of mammals. Proc Siberian Branch USSR Acad Sci. 1983:10:115–119.

Graphodatsky AS, Perelman PL, O'Brien SJ. Atlas of mammalian chromosomes. John Wiley & Sons; 2020.

Graphodatsky AS, Sharshov AA, Ternovsky DV, Ternovskaya YG. Comparative cytogenesis of Mustelidae (Carnivora). Zool J. 1989:68:96–106.

Graphodatsky AS, Ternovskaya YG, Ternovsky DV. Distribution of structural heterochromatin and the nucleolar organizer regions in the chromosomes of Siberian polecat, mink, and their hybrids. Proc Acad Sci. 1982:262:460–461.

Graphodatsky AS, Ternovskaya YG, Ternovsky DV. Formation of the new nucleolus organizer regions in the European mink/polecats hybrids. Genetika. 1985:21:640–645.

Graphodatsky AS, Ternovsky DV, Isaenko AA, Radzhabli SI. Constitutive heterochromatin and DNA content in some Mustelids (Mustelidae, Carnivora). Genetika. 1977:13:2123–2128.

Graphodatsky AS, Volobuev VT, Ternovsky DV, Radzhabli SI. G-banding of the chromosomes in seven species of Mustelidae (Carnivora). Zool J. 1976:55:1704–1709.

Guan D, et al. Identifying and removing haplotypic duplication in primary genome assemblies. Bioinformatics. 2020:36:2896–2898. https://doi.org/10.1093/bioinformatics/btaa025.

Hardie DC, Gregory TR, Hebert PDN. From pixels to picograms: a beginners' guide to genome quantification by feulgen image analysis densitometry. J Histochem Cytochem. 2002:50:735–749. https://doi.org/10.1177/002215540205000601.

Harding LE, Smith FA. Mustela or vison? Evidence for the taxonomic status of the American mink and a distinct biogeographic radiation of American weasels. Mol Phylogenet Evol. 2009:52:632–642. https://doi.org/10.1016/j.ympev.2009.05.036.

Harrington LA, Marino J, King CM. People and wild musteloids. In: Macdonald DW, Newman C, Harrington LA, editors. Biology and conservation of musteloids. Oxford University Press; 2017. p. 189–215.

Hassanin A, et al. Evolutionary history of Carnivora (Mammalia, Laurasiatheria) inferred from mitochondrial genomes. PLoS One. 2021:16:e0240770. https://doi.org/10.1371/journal.pone.0240770.

Hayder F, Madikiza ZJK, San EDL. Updated distribution and current population Status of the Least Weasel (Mustela nivalis) in Tunisia: a countrywide interview survey. Afr J Wildl Res. 2023:53:11–18. https://doi.org/10.3957/056.053.0011.

Hiller TL, Vantassel SM. The global consumptive use of small carnivores: social, cultural, religious, economic, and subsistence trends from prehistoric to modern times. In: Small carnivores: evolution, ecology, behaviour, and conservation. John Wiley & Sons; 2022. p. 489–507.

Hoeppner MP, et al. An improved canine genome and a comprehensive catalogue of coding genes and non-coding transcripts. PLoS One. 2014:9:e91172. https://doi.org/10.1371/journal.pone.0091172.

Huerta-Cepas J, Serra F, Bork P. ETE 3: reconstruction, analysis, and visualization of phylogenomic data. Mol Biol Evol. 2016:33:1635–1638. https://doi.org/10.1093/molbev/msw046.

IUCN. The IUCN Red List of threatened species. Version 2025-1. [updated 2025 Apr 30]. https://www.iucnredlist.org/en.

Jachowski D, Kays R, Butler A, Hoylman AM, Gompper ME. Tracking the decline of weasels in North America. PLoS One. 2021:16:e0254387. https://doi.org/10.1371/journal.pone.0254387.

Kinoshita E, et al. Hybridization between the European and Asian badgers (Meles, Carnivora) in the Volga-Kama region, revealed by analyses of maternally, paternally and biparentally inherited genes. Mamm Biol. 2019:94:140–148. https://doi.org/10.1016/j.mambio.2018.05.003.

Kiseleva NV. Depression of the population of the steppe polecat (*Mustela eversmanii*) in the Southern Urals. Biol Bull. 2024:51:463–471. https://doi.org/10.1134/S1062359023602999.

Kitchener AC, Meloro C, Williams TM. Form and function of the musteloids. In: Macdonald DW, Newman C, Harrington LA, editors. Biology and conservation of Musteloids. Oxford University Press; 2017. p. 98–135.

Kliver S, et al. Comparative genomics of Caniformia revealed an ancient burst of inversions prior to the radiation of Mustelidae. Prep; 2026.

Kliver S, Tamazian G, Brukhin V, O'brien S, Kommisarov A. KrATER: K-mer Analysis Tool Easy to Run. Proceedings of 8th International Moscow Conference. Moscow: IITP RAS. p. 128. 2017.

Koepfli K-P, et al. Multigene phylogeny of the Mustelidae: resolving relationships, tempo and biogeographic history of a mammalian adaptive radiation. BMC Biol. 2008a:6:10. https://doi.org/10.1186/1741-7007-6-10.

Koepfli K-P, et al. Establishing the foundation for an applied molecular taxonomy of otters in Southeast Asia. Conserv Genet. 2008b:9:1589–1604. https://doi.org/10.1007/s10592-007-9498-5.

Kosintsev PA, Gasilin VV, Gimranov DO, Bachura OP. Carnivores (Mammalia, Carnivora) of the Urals in the Late Pleistocene and Holocene. Quat Int. 2016:420:145–155. https://doi.org/10.1016/j.quaint.2015.10.089.

Kozlov O, Morel B, Barbera P, computations, Redelings B. 2024, April 30. amkozlov/raxml-ng: RAxML-NG v1.2.2. Version 1.2.2. [Computer software]. Zenodo. https://doi.org/10.5281/zenodo.11095121.

Krajcarz MT, Krajcarz M, Goslar T, Nadachowski A. The first radiocarbon dated steppe polecat (*Mustela eversmanii*) from the Pleistocene of Poland. Quat Int. 2015:357:237–244. https://doi.org/10.1016/j.quaint.2014.06.001.

Krasheninnikova K, et al. halSynteny: a fast, easy-to-use conserved synteny block construction method for multiple whole-genome alignments. GigaScience. 2020:9:giaa047. https://doi.org/10.1093/gigascience/giaa047.

Kuraku S, Zmasek CM, Nishimura O, Katoh K. Aleaves facilitates on-demand exploration of metazoan gene family trees on MAFFT sequence alignment server with enhanced interactivity. Nucleic Acids Res. 2013:41:W22–W28. https://doi.org/10.1093/nar/gkt389.

Lande R, Shannon S. The role of genetic variation in adaptation and population persistence in a changing environment. Evolution. 1996:50:434–437. https://doi.org/10.1111/j.1558-5646.1996.tb04504.x.

Law CJ, Slater GJ, Mehta RS. Lineage diversity and size disparity in Musteloidea: testing patterns of adaptive radiation using molecular and fossil-based methods. Syst Biol. 2018:67:127–144. https://doi.org/10.1093/sysbio/syx047.

Lebarbenchon C, Poitevin F, Arnal V, Montgelard C. Phylogeography of the weasel (*Mustela nivalis*) in the western-Palaearctic region: combined effects of glacial events and human movements. Heredity (Edinb). 2010:105:449–462. https://doi.org/10.1038/hdy.2009.186.

Li H, et al. The sequence alignment/map format and SAMtools. Bioinformatics. 2009:25:2078–2079. https://doi.org/10.1093/bioinformatics/btp352.

Li H. A statistical framework for SNP calling, mutation discovery, association mapping and population genetical parameter estimation from sequencing data. Bioinformatics. 2011:27:2987–2993. https://doi.org/10.1093/bioinformatics/btr509.

Li H, Durbin R. Fast and accurate short read alignment with burrows–wheeler transform. Bioinformatics. 2009:25:1754–1760. https://doi.org/10.1093/bioinformatics/btp324.

Li H, Durbin R. Inference of human population history from individual whole-genome sequences. Nature. 2011:475:493–496. https://doi.org/10.1038/nature10231.

Liu Y, et al. Revalidation and expanded description of *Mustela aistoodonnivalis* (Mustelidae: Carnivora) based on a multigene phylogeny and morphology. Ecol Evol. 2023:13:e9944. https://doi.org/10.1002/ece3.9944.

Llorca AB, Tortosa FS, Guerrero-Casado J. Lack of data or lack of weasels? The likely silent extinction of Weasel *Mustela nivalis* (Carnivora: Mustelidae) in Spain. Diversity (Basel). 2024:16:446. https://doi.org/10.3390/d16080446.

Lomanov IK, et al. Status of resources game animals in Russian Federation 2003-2007. Information and analytical materials. Game animals of Russia (biology, protection, study of resources, rational use). Moscow, FGU Centrokhotkontrol. 8:164. 2007.

Macdonald DW, Harrington LA. The American mink: the triumph and tragedy of adaptation out of context. N Z J Zool. 2003:30:421–441. https://doi.org/10.1080/03014223.2003.9518350.

Macdonald DW, Harrington LA, Newman C. Dramatis personae: an introduction to the wild musteloids. In: Macdonald DW, Newman C, Harrington LA, editors. Biology and conservation of Musteloids. Oxford University Press; 2017. p. 3–74.

Marçais G, Kingsford C. A fast, lock-free approach for efficient parallel counting of occurrences of *k*-mers. Bioinformatics. 2011:27:764–770. https://doi.org/10.1093/bioinformatics/btr011.

Marciszak A, Socha P. Stoat *Mustela erminea* Linnaeus, 1758 and weasel *Mustela nivalis* Linnaeus, 1766 in palaeoecological analysis: a case study of Biśnik Cave. Quat Int. 2014:339–340: 258–265. https://doi.org/10.1016/j.quaint.2013.12.058.

McDevitt AD, et al. Individual variation in dispersal associated with phenotype influences fine-scale genetic structure in weasels. Conserv Genet. 2013:14:499–509. https://doi.org/10.1007/s10592-012-0376-4.

Minprirody of Russia. State report "On the State and Environmental Protection of the Russian Federation in 2023." Ministry of Natural Resources and Environment of the Russian Federation. [updated 2024 Nov 7]. https://2023.ecology-gosdoklad.ru/.

Miranda I, et al. Museomics dissects the genetic basis for adaptive seasonal coloration in the least weasel. Mol Biol Evol. 2021:38: 4388–4402. https://doi.org/10.1093/molbev/msab177.

Morgulis A, Gertz EM, Schäffer AA, Agarwala R. WindowMasker: window-based masker for sequenced genomes. Bioinforma Oxf Engl. 2006:22:134–141. https://doi.org/10.1093/bioinformatics/bti774.

Nash WG, et al. The ancestral carnivore karyotype (2n=38) lives today in ringtails. J Hered. 2008:99:241–253. https://doi.org/10.1093/jhered/esm130.

O'Brien MF, et al. The genome sequence of the least weasel, *Mustela nivalis* Linnaeus, 1766 (Carnivora: Mustelidae) [version 1; peer review: 1 approved, 1 approved with reservations]. Wellcome Open Res. 2025:10:488. https://doi.org/10.12688/wellcomeopenres.24862.1.

Paradis E, Schliep K. Ape 5.0: an environment for modern phylogenetics and evolutionary analyses in R. Bioinformatics. 2019:35:526–528. https://doi.org/10.1093/bioinformatics/bty633.

Patterson BD, Chaves HER, Soares AER, Vilela JF, Grewe F. Complete mitochondrial genomes support the composition and rank of the American weasel genus Neogale (Carnivora: Mustelidae). J Anim Divers. 2025:7:41–48. https://doi.org/10.22034/JAD.2025.7.1.3.

Patterson BD, Ramírez-Chaves HE, Vilela JF, Soares AER, Grewe F. On the nomenclature of the American clade of weasels (Carnivora: Mustelidae). J Anim Divers. 2021:3:1–8. https://doi.org/10.52547/JAD.2021.3.2.1.

Pedersen BS, Quinlan AR. Mosdepth: quick coverage calculation for genomes and exomes. Bioinformatics. 2018:34:867–868. https://doi.org/10.1093/bioinformatics/btx699.

Perelman PL, et al. Comparative chromosome painting in Carnivora and Pholidota. Cytogenet Genome Res. 2012:137:174–193. https://doi.org/10.1159/000341389.

Peters SE, McClennen M. The paleobiology database application programming interface. Paleobiology. 2016:42:1–7. https://doi.org/10.1017/pab.2015.39.

Quinlan AR, Hall IM. BEDTools: a flexible suite of utilities for comparing genomic features. Bioinformatics. 2010:26:841–842. https://doi.org/10.1093/bioinformatics/btq033.

Ranallo-Benavidez TR, Jaron KS, Schatz MC. GenomeScope 2.0 and Smudgeplot for reference-free profiling of polyploid genomes. Nat Commun. 2020:11:1432. https://doi.org/10.1038/s41467-020-14998-3.

Rao SSP, et al. A 3D map of the human genome at kilobase resolution reveals principles of chromatin looping. Cell. 2014:159: 1665–1680. https://doi.org/10.1016/j.cell.2014.11.021.

Robinson JA, et al. Genomic flatlining in the endangered Island Fox. Curr Biol. 2016:26:1183–1189. https://doi.org/10.1016/j.cub.2016.02.062.

Robinson JA, et al. Genomic signatures of extensive inbreeding in Isle Royale wolves, a population on the threshold of extinction. Sci Adv. 2019:5:eaau0757. https://doi.org/10.1126/sciadv.aau0757.

Rozhnov VV, Pishchulina SL, Meschersky IG, Simakin LV. On the ratio of phenotype and genotype of sable and pine marten in sympatry zone in the Northern Urals. Mosc Univ Biol Sci Bull. 2013:68: 178–181. https://doi.org/10.3103/S009639251304007X.

Sainsbury KA, et al. Recent history, current status, conservation and management of native mammalian carnivore species in Great Britain. Mammal Rev. 2019:49:171–188. https://doi.org/10.1111/mam.12150.

Šálek M, et al. Population status, habitat associations, and distribution of the steppe polecat *Mustela eversmanii* in Europe. Acta Theriol (Warsz). 2013:58:233–244. https://doi.org/10.1007/s13364-013-0134-0.

Sambrook J, Russell DW. Purification of nucleic acids by extraction with phenol:chloroform. Cold Spring Harb Protoc. 2006:2006: pdb.prot4455. https://doi.org/10.1101/pdb.prot4455.

Sato JJ, et al. Evolutionary and biogeographic history of weasel-like carnivorans (Musteloidea). Mol Phylogenet Evol. 2012:63: 745–757. https://doi.org/10.1016/j.ympev.2012.02.025.

Sato T, et al. Phylogeography and population history of the least weasel (*Mustela nivalis*) in the Palearctic based on multilocus analysis. J Zool Syst Evol Res. 2020:58:408–426. https://doi.org/10.1111/jzs.12330.

Schneider VA, et al. Evaluation of GRCh38 and de novo haploid genome assemblies demonstrates the enduring quality of the reference assembly. Genome Res. 2017:27:849–864. https://doi.org/10.1101/gr.213611.116.

Sedlazeck FJ, Lee H, Darby CA, Schatz MC. Piercing the dark matter: bioinformatics of long-range sequencing and mapping. Nat Rev Genet. 2018:19:329–346. https://doi.org/10.1038/s41576-018-0003-4.

Shaw R, MacPherson J, Kitchener AC, Etherington GJ, Haerty W. Characterisation of the historic demographic decline of the British European polecat population. Mol Ecol. 2025:34: e70091. https://doi.org/10.1111/mec.70091.

Shilova SA. Abundance control and conservation of sousliks in Russia (*G. spermophilus*). Arid Ecosyst. 2011:1:267–272. https://doi.org/10.1134/S2079096111040147.

Simonsen M, Mailund T, Pedersen CNS. Rapid neighbour-joining. In: Crandall KA, Lagergren J, editors. Algorithms in bioinformatics. Springer; 2008. p. 113–122.

Simpson GG. The principles of classification and a classification of mammals. New York: Bulletin of the American Museum of Natural History. 1945. p. 1–367.

Sommer R, Benecke N. Late- and post-glacial history of the Mustelidae in Europe. Mamm Rev. 2004:34:249–284. https://doi.org/10.1111/j.1365-2907.2004.00043.x.

Sommer RS, Crees JJ. Late quaternary biogeography of small carnivores in Europe. In: Do Linh San E, Sato JJ, Belant JL, Somers MJ, editors. Small carnivores: evolution, ecology, behaviour, and Conservation. John Wiley & Sons; 2022. p. 79–91.

Szapu JS, Cserkész T, Pirger Z, Kiss C, Lanszki J. Exposure to anticoagulant rodenticides in steppe polecat (*Mustela eversmanii*) and European polecat (*Mustela putorius*) in central Europe. Sci Total Environ. 2024:948:174282. https://doi.org/10.1016/j.scitotenv.2024.174282.

Szatmári L, et al. A comparison of microsatellites and genome-wide SNPs for the detection of admixture brings the first

molecular evidence for hybridization between *Mustela eversmanii* and *M. putorius* (Mustelidae, Carnivora). Evol Appl. 2021:14:2286–2304. https://doi.org/10.1111/eva.13291.
Tarailo-Graovac M, Chen N. Using RepeatMasker to identify repetitive elements in genomic sequences. Curr Protoc Bioinforma. 2009:25:4.10.1–4.10.14. https://doi.org/10.1002/0471250953.bi0410s25.
Teixeira JC, Huber CD. The inflated significance of neutral genetic diversity in conservation genetics. Proc Natl Acad Sci U S A. 2021:118:e2015096118. https://doi.org/10.1073/pnas.2015096118.
Theissinger K, et al. How genomics can help biodiversity conservation. Trends Genet. 2023:39:545–559. https://doi.org/10.1016/j.tig.2023.01.005.
Tissaoui G, et al. Evolutionary characteristics of the mitochondrial NADH dehydrogenase subunit 6 gene in some populations of four sympatric *Mustela* species (Mustelidae, Mammalia) from central Europe. Mol Biol Rep. 2024:51:575. https://doi.org/10.1007/s11033-024-09505-6.
Tomarovsky AA, et al. Genomics of sable (*Martes zibellina*) × pine marten (*Martes martes*) hybridization. bioRxiv 668050. https://doi.org/10.1101/2025.08.01.668050, 2 August 2025, preprint: not peer reviewed.
Totikov A, et al. Chromosome-level genome assemblies expand capabilities of genomics for conservation biology. Genes (Basel). 2021:12:1336. https://doi.org/10.3390/genes12091336.
Van der Auwera GA, et al. From FastQ data to high-confidence variant calls: the genome analysis toolkit best practices pipeline. Curr Protoc Bioinforma. 2013:43:11.10.1–11.10.33. https://doi.org/10.1002/0471250953.bi1110s43.
Vass G, Bende A. Morphometric characteristics of the Weasel (*Mustela nivalis* L.) in the light of literature data. Magy Apróvad Közlemények. 2023:15:107–126. https://doi.org/10.17243/mavk.2023.107.
Vazhov SV, Bachtin RF, Vazhov VM. On entering the red-cheeked ground squirrel in the red book of Altai territory. Int J Fund Appl Res. 2016:599:500–503.
Wick RR, Judd LM, Gorrie CL, Holt KE. Completing bacterial genome assemblies with multiplex MinION sequencing. Microb Genomics. 2017:3:e000132. https://doi.org/10.1099/mgen.0.000132.
Wright PGR, Croose E, Macpherson JL. A global review of the conservation threats and status of mustelids. Mammal Rev. 2022:52:410–424. https://doi.org/10.1111/mam.12288.
Yu L, et al. On the phylogeny of Mustelidae subfamilies: analysis of seventeen nuclear non-coding loci and mitochondrial complete genomes. BMC Evol Biol. 2011:11:92. https://doi.org/10.1186/1471-2148-11-92.
Zhang C, Rabiee M, Sayyari E, Mirarab S. ASTRAL-III: polynomial time species tree reconstruction from partially resolved gene trees. BMC Bioinformatics. 2018:19:153. https://doi.org/10.1186/s12859-018-2129-y.
Zimin AV, et al. The MaSuRCA genome assembler. Bioinformatics. 2013:29:2669–2677. https://doi.org/10.1093/bioinformatics/btt476.
Zimin AV, Salzberg SL. The genome polishing tool POLCA makes fast and accurate corrections in genome assemblies. PLOS Comput Biol. 2020:16:e1007981. https://doi.org/10.1371/journal.pcbi.1007981.
Zimin AV, Salzberg SL. The SAMBA tool uses long reads to improve the contiguity of genome assemblies. PLoS Comput Biol. 2022:18:e1009860. https://doi.org/10.1371/journal.pcbi.1009860.

Associate editor: Diego Ortega-Del Vecchyo